The FEBS Journal

FEBS PRESS science publishing by scientists

Enhanced expression of HNF4α during intestinal epithelial differentiation is involved in the activation of ER stress

Sinem Tunçer[1], Aslı Sade-Memişoğlu[1], Ayşe Gökçe Keşküş[2], Ilir Sheraj[1], Güneş Güner[3], Aytekin Akyol[3] and Sreeparna Banerjee[1,4]

1 Department of Biological Sciences, Orta Dogu Teknik Universitesi, Ankara, Turkey
2 Department of Molecular Biology and Genetics, Bilkent University, Ankara, Turkey
3 Department of Pathology, Faculty of Medicine, Hacettepe University, Ankara, Turkey
4 Department of Biological Sciences and Cancer Systems Biology Laboratory (CanSyl), Orta Dogu Teknik Universitesi, Ankara, Turkey

Keywords
ATF6; autophagy; colon; differentiation; ER stress; HNF4α; XBP1

Correspondence
S. Banerjee, Department of Biological Sciences, Orta Dogu Teknik Universitesi (ODTU/METU), Ankara 06800, Turkey
Tel: +90 312 210 6468
E-mail: banerjee@metu.edu.tr

Present address
Vocational School of Health Services, Department of Medical Laboratory Techniques, and Biotechnology Application and Research Center, Bilecik Şeyh Edebali University, Bilecik, Turkey
Department of Science Education, Dokuz Eylul University, Izmir, Turkey
Mardin State Hospital, Mardin, Turkey

(Received 20 July 2019, revised 17 October 2019, accepted 21 November 2019)

doi:10.1111/febs.15152

Intestinal epithelial cells are derived from stem cells at the crypts that undergo differentiation into transit-amplifying cells, which in turn form terminally differentiated enterocytes as these cells reach the villus. Extensive alterations in both transcriptional and translational programs occur during differentiation, which can induce the activation of cellular stress responses such as ER stress-related unfolded protein response (UPR) and autophagy, particularly in the cells that are already committed to becoming absorptive cells. Using an epithelial cell model of enterocyte differentiation, we report a mechanistic study connecting enterocyte differentiation to UPR and autophagy. We report that differentiated colon epithelial cells showed increased cytosolic Ca^{2+} levels and activation of all three pathways of UPR: inositol-requiring enzyme 1 (IRE1), protein kinase RNA-like ER kinase, and activating transcription factor 6 (ATF6) compared to the undifferentiated cells. Enhanced UPR in the differentiated cells was accompanied by the induction of autophagy as evidenced by increased ratio of light chain 3 II/I, upregulation of Beclin-1, and downregulation of p62. We show for the first time that mechanistically, the upregulation of hepatocyte nuclear factor 4α (HNF4α) during differentiation led to increased promoter binding and transcriptional upregulation of two major proteins of UPR: X-box binding protein-1 and ATF6, implicating HNF4α as a key regulator of UPR response during differentiation. Integrating wet-lab with *in silico* analyses, the present study links differentiation to cellular stress responses, and highlights the importance of transcription factor signaling and cross-talk between the cellular events in the regulation of intestinal cell differentiation.

Introduction

The intestinal epithelium consists of a polarized monolayer of columnar epithelial cells, goblet cells that secrete mucus, Paneth cells that have immune regulatory functions, and enteroendocrine cells that secrete hormones necessary to coordinate digestion and absorption [1]. All of these cells are highly

Abbreviations
ALP, alkaline phosphatase; AMPK, AMP-activated protein kinase; ATF6, activating transcription factor 6; ATG, autophagy-related; CEA, carcinoembryonic antigen; DAB, diaminobenzidine; DAPK1, death-associated protein kinase-1; eIF2α, eukaryotic initiation factor 2α; GO, Gene Ontology; HNF4α, hepatocyte nuclear factor 4α; IRE1, inositol-requiring enzyme 1; mTOR, mammalian target of rapamycin; PERK, protein kinase RNA-like endoplasmic reticulum kinase; SERCA, sarco/endoplasmic reticulum Ca^{2+} ATPase; SI, sucrose isomaltase; TA, transit-amplifying; TET, ten-eleven translocation family of enzymes; TG, thapsigargin; TMA, tissue microarray; TN, tunicamycin; TSS, transcription start site; UPR, unfolded protein response; XBP1, X-box binding protein-1.

differentiated and are generated from Lgr^{5+} intestinal stem cells that reside in the crypt [2]. The stem cells give rise to committed transit-amplifying (TA) cells that migrate upwards from the crypt as they undergo cell division. At the crypt–villus junction, proliferation of the epithelial cells ceases and they differentiate into absorptive cells [3]. During the process of cellular differentiation, large volumes of transmembrane and secretory proteins are processed in the ER, leading to the activation of an ER stress response called the unfolded protein response (UPR) that is important for the maintenance of homeostasis [4]. Three principal arms of the UPR have been identified: activating transcription factor 6 (ATF6), inositol-requiring enzyme 1 (IRE1), and double-stranded RNA-dependent protein kinase (PKR)-like ER kinase (PERK). ATF6 is a type II transmembrane protein; under ER stress, its cytosolic amino-terminal segment undergoes proteolysis and it functions as a transcription factor that induces the expression of UPR target genes including those encoding chaperones and other transcription factors such as X-box binding protein 1 (XBP1). As one of the IRE1 paralogs in mammals, IRE1α is ubiquitously expressed and is required for XBP1 mRNA splicing. The translation product of the spliced XBP1, XBP1s, induces the expression of components of ER-associated degradation [5,6]. PERK possesses a luminal sensor domain and a cytosolic effector domain with kinase activity. During ER stress, PERK phosphorylates eukaryotic initiation factor 2α (eIF2α), at Ser 51; this is an inhibitory phosphorylation that transiently suppresses global translation initiation while inducing the selective translation of ATF4 that upregulates UPR target genes [6].

Induction of ER stress has been shown to be higher in the more differentiated TA cells compared to the stem cells in the intestinal crypts, suggesting that ER stress can play a role in intestinal stem cell fate and decision to differentiate [7]. In a high-throughput study using a systems biology approach, hepatocyte nuclear factor 4α (HNF4α) was identified as a crucial transcription factor that was highly enriched at the promoters of genes that are expressed in the intestinal villi, as compared to the crypt or embryonic endoderm [3]. HNF4 α is a highly conserved orphan receptor that belongs to the nuclear hormone receptor superfamily and is expressed in the mucosal epithelial cells of the gastrointestinal tract (intestine/colon, stomach), liver, kidney, and pancreas. It transcriptionally regulates the expression of various genes and functions in various processes such as intestinal cellular differentiation during endoderm development and in the adult, as well as the metabolism of nutrients and drugs, and epithelial polarization [8]. Interestingly, in pancreatic beta cells as well as gastric epithelial cells, HNF4α was shown to enhance the expression of XBP1 [9,10].

The presence of ER stress often leads to the induction of macroautophagy (hereafter referred to as autophagy). Autophagy involves the formation of isolation membranes eventually generating double-membraned vesicles called autophagosomes that contain cytosolic components including organelles. The autophagosomes fuse with lysosomes, leading to the degradation of cytosolic components [11]. The ER can provide a scaffold for the formation of autophagosomes, potentially at sites where the mitochondria contact the ER, generating a cradle from which the isolation membrane extrudes and recruits a number of autophagy-related proteins (ATGs). As the autophagosome matures, a key ATG8 family of proteins called the microtubule-associated protein 1A/1B-light chain 3 (LC3) A, B, and C is recruited and lipidated yielding LC3-II, which is then covalently attached to nascent autophagosomal membranes [12]. Therefore, the LC3-II-to-LC3-I ratio is broadly used as a reliable index of autophagy [13]. Autophagy may be nonspecific, or it may specifically target damaged organelles, protein aggregates, or pathogens with the aim to restore homeostasis. The choice of the 'cargo' depends on the cargo receptors, for example, p62/SQSTM1 is a receptor protein that can link cargo to ATG8, such as during the autophagic removal of protein aggregates [14,15].

In the presence of bacterial invasion, Paneth cells of the gut were shown to undergo ER stress leading to secretory autophagy whereby LC3-positive autophagosomes were used to secrete lysozyme (important for antibacterial defense) rather than fuse with the lysosome [16]. Gut epithelial cells, which are known to participate in immunological reactions [17], have been shown to undergo autophagy in response to bacterial secretory products as a stress response [18]. Additionally, autophagy resulting from nutrient starvation was shown to enhance barrier function by reducing the expression of a pore-forming protein claudin-1 [19]. We have previously reported that Caco-2 cells can undergo autophagy even in the absence of nutrient starvation during contact inhibition-mediated spontaneous differentiation [13]. In the current study, we have aimed to better understand the mechanism for the induction of ER stress, UPR, and subsequent autophagy in the course of enterocyte-like differentiation of colon epithelial cells. We report for the first time that the expression of HNF4α in terminally differentiated colon epithelial cells was associated with the upregulation of XBP1 and ATF6; this in turn led to the activation of UPR and upregulation of various

ER stress markers. Here, we demonstrate a novel regulatory node involving HNF4α, which links ER stress to intestinal enterocyte differentiation.

Results

Enhanced expression of HNF4α in differentiated colon epithelial cells

It is known that the differentiation of secretory cells in the villus of the small intestine of mice is closely regulated by the transcription factors Hnf4α and Cdx2 [20]. Additionally, the expression of HNF4α has been reported to be increased in confluent Caco-2 cells when compared to preconfluent cells [21]. To examine whether the HNF4α expression increased in the course of differentiation, we first confirmed the induction of differentiation in Caco-2 cells. Caco-2 cells were collected during their proliferative phase (subconfluent), as well as on days 0, 10, and 20 after attaining 100% confluence. Along with enhanced dome formation [13] (Fig. 1A), differentiation was confirmed by enhanced expression of differentiation markers sucrase isomaltase (SI) (Fig. 1B), enhanced expression, and activity of alkaline phosphatase (ALP) [22] (Fig. 1C), and increase in E-cadherin expression [22] (Fig. 1D). In

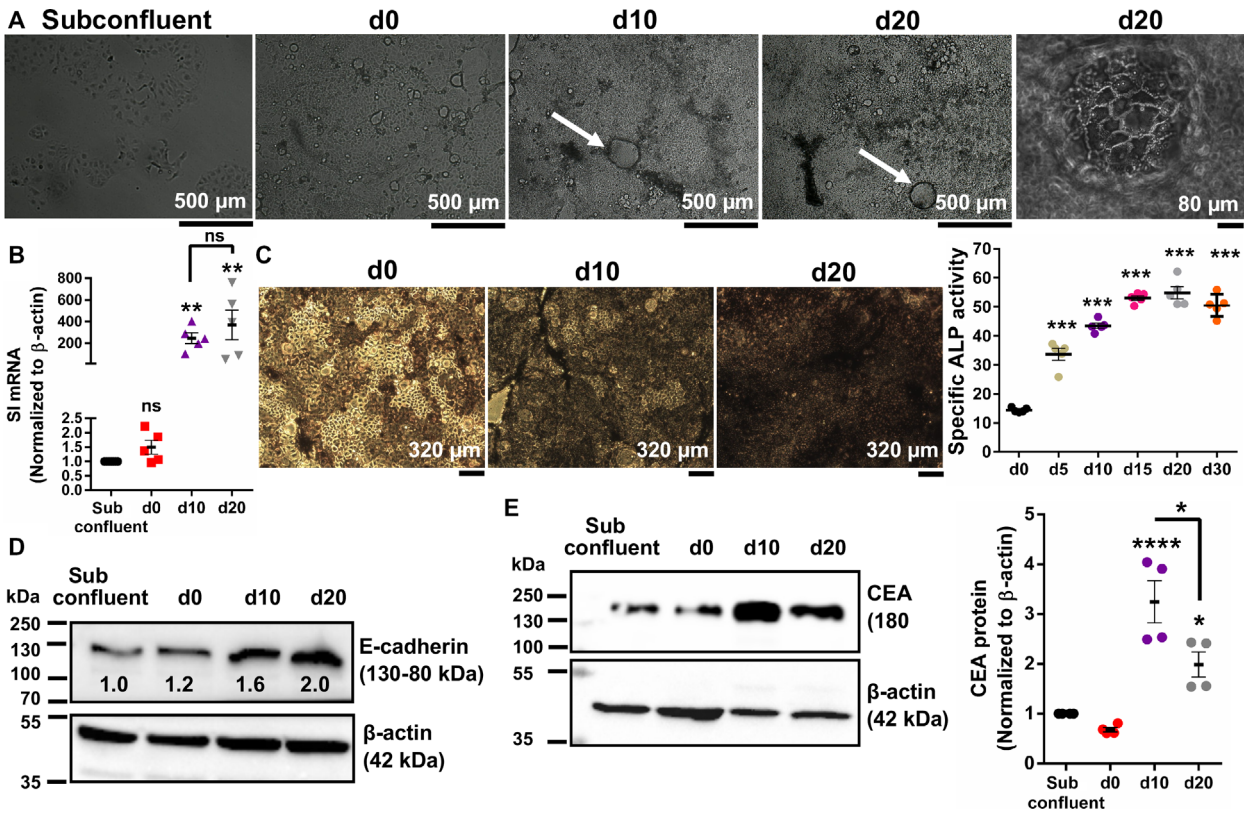

Fig. 1. Confirmation of differentiation in Caco-2 cells: (A) Caco-2 cells were assessed using an inverted light microscope for morphological changes during spontaneous differentiation. Representative images are given for subconfluent cells, confluent (day 0) cells, and differentiated cells collected 10 and 20 days after reaching confluency. Domes in the differentiated cells are shown with arrows. The brightness and contrast of the image were artificially adjusted to ensure maximum visibility of the cells. (B) SI expression was observed to increase in spontaneously differentiating Caco-2 cells (n = 5; each with three technical replicates). The results are given as mean ± SEM. t-Test was used to compare d0 or differentiated cells with undifferentiated (subconfluent) cells (ns = not significant; $^{**}P \leq 0.01$). (C) ALP activity was determined by a spectrophotometric assay using pNPP phosphatase (right panel) and also by staining the cells with NBT/BCIP substrate which generates an intense black-purple precipitate at the site of ALP binding. Higher ALP expression in the differentiated cells is reflected by the darker color of the precipitate (left panel). Scale bars represent 320 µm for each microscope images. The results are shown as mean ± SEM (n = 5). t-Test was used to compare the means with d0 cells and for statistical significance ($^{***}P \leq 0.001$). (D) Western blot showing an increase in E-cadherin expression in the spontaneously differentiated Caco-2 cells (representative image of two biological replicates). (E) Western blot showing an increase in the expression of CEA in the spontaneously differentiated Caco-2 cells. Graph shows the mean ± SEM from four independent replicates, and t-test was used for comparison with subconfluent cells ($^{*}P \leq 0.05$ and $^{****}P \leq 0.0001$).

addition, cell density-dependent increase in expression of carcinoembryonic antigen (CEA) [23] was observed in postconfluent Caco-2 cells (Fig. 1E).

The differentiated Caco-2 cells showed increased protein expression of HNF4α and CDX2 in the nuclear protein fraction (Fig. 2A) and total protein extract (Fig. 2B, upper panel). A combination of alternative splicing and alternative promoter usage is known to generate ten different HNF4α isoforms (GRCh38.p7 Primary Assembly, NCBI) (Table S1). Isoforms produced by the activity of the proximal promoter are referred to as P1, whereas isoforms produced by the more distal promoter are designated as P2 [24]. These two isoform classes differ in both their N and C termini [25]. Therefore, HNF4α expression during spontaneous differentiation of Caco-2 cells was examined with two different HNF4α antibody clones: clone C-19, which can recognize isoforms 1, 2, 4, 5, 7, 8, and 9, and clone K9218, which can detect isoforms 1, 2, and 3 [26]. We have observed enhanced expression of HNF4α with both antibodies (Fig. 2B, lower panel). We also examined the mRNA expression of *HNF4α* by using primers designed on the basis of the region conserved in all isoforms (Fig. 2C, left panel) and expression profiles of both P1 (transcript variants 1, 2, 3, and 7) and P2 transcripts (transcript variants 4, 5, 6, 8, 9, and 10) (Fig. 2C, right panel) during spontaneous differentiation of Caco-2 cells. mRNA expression of transcripts 7, 8, 9, and 10 was not detected in undifferentiated or differentiated Caco-2 cells (data not shown). We found that although expression of both P1 transcripts (transcript variants 1, 2, and 3) and P2 transcripts (transcript variants 4, 5, and 6) were increasing during the differentiation, the level of increase in the expression of P1 variants was more prominent. Further analysis of a microarray dataset (GSE84742) [27] consisting of data from murine cells collected from distal colon crypt base (undifferentiated) and luminal surface (differentiated) confirmed that the expression of *Hnf4α* was higher in differentiated surface epithelia (Fig. 2D).

To determine whether the expression of HNF4α also differed according to the state of differentiation of colorectal (CRC) tumor samples, we used four tissue microarrays (TMA) consisting of a total of 202 CRC cases and 14 normal samples. We observed that most of the normal colonic epithelial cells ($n = 14$ spots) had weak HNF4α staining (12/14), while two (2/14) displayed strong HNF4α staining. The staining for CDX2, a known target of HNF4α as well as a transcriptional binding partner, was positive in most samples (12/14) and strong positive in two (2/14). The tumors were grouped into two major classes based on their differentiation status: low-grade (well-differentiated and moderately differentiated; grades 1 and 2, respectively) and high-grade (poorly differentiated and undifferentiated; grades 3 and 4, respectively) (Fig. 2E). In the tumor samples, a significant (Pearson chi-square test) association was observed between the degree of differentiation and the expression of both HNF4α ($P = 0.041$) and CDX2 ($P = 0.029$). No association was seen for the expression of two unrelated proteins p53 ($P = 0.275$) and cathepsin E (CTSE; $P = 0.438$). The expressions of HNF4α and CDX2 were also highly correlated to each other in the tumor samples ($n = 188$, $r = 0.405$, $P = 0.000$, Kendall rank correlation).

Enhanced hydroxymethylation of the *HNF4α* promoter by ten-eleven translocation family of enzymes (TET) dioxygenases was reported in terminal hepatocyte differentiation, which could contribute to the increased expression of HNF4α observed in these cells [28]. To determine whether a similar mechanism was responsible for the increased expression of HNF4α during terminal differentiation of colon epithelial cells, 5.0 kb upstream and 5.0 kb downstream regions of the transcription start site (TSS) [29] of P1 and P2 transcripts were analyzed for cytosine hydroxymethylation in differentiated and undifferentiated T84 cells (GSE69333) [30]. T84 is a colon carcinoma epithelial cell line that can also undergo differentiation spontaneously after reaching 100% confluency [31]. In accordance with the increased expression of HNF4α mRNA (Fig. 2C), we observed enhanced cytosine hydroxymethylation in the analyzed regions for both P1 and P2 transcripts in the course of differentiation (peak fold enrichments with the smallest q values are as follows: at day 12, fold change for P2 promoter = 4.6, $q = 0.019$ and P1 fold change = 5.8, $q = 0.0017$; at day 15, fold change for P2 promoter = 4.3, $q = 2.3E\text{-}4$ and P1 fold change = 8.5, $q = 4.37E\text{-}15$) (Fig. 2F). Of note, increase in hydroxymethylation in the differentiated cells compared to undifferentiated cells was also identified beyond the 5.0 kb downstream (intragenic region) of the TSS (Table S2).

HNF4α transcriptionally upregulates *XBP1* and *ATF6* during intestinal epithelial differentiation

To determine the targets of HNF4α in differentiated and undifferentiated Caco-2 cells, we analyzed a publicly available HNF4α ChIP-sequencing dataset (GSE23436) using proliferating and differentiated Caco-2 cells [32]. Gene Ontology (GO) was used to perform enrichment analysis on the genes in which the promoters are significantly occupied by HNF4α in both differentiated and undifferentiated cells. We

specifically chose to examine the GO terms related to differentiation, ER stress, and autophagy as we have previously shown that spontaneously differentiated Caco-2 cells can undergo autophagy even in the absence of nutrient starvation [13]. We observed statistically significant enrichment of the GO terms 'cell differentiation GO:0030154', 'response to ER stress GO:0034976', and 'autophagy GO:0006914' in the HNF4α binding sequences in both undifferentiated and differentiated Caco-2 cells (Fig. 3A). We next sought to understand whether there were any common genes in all three GO terms that were regulated by HNF4α. Two genes were in common for both differentiated and undifferentiated cells in the three GO terms: *XBP1* and *PARK2*. HNF4α recruitment to the promoter of *PARK2* did not change with differentiation; however, the recruitment of HNF4α to the promoter of *XBP1* was significantly higher in the differentiated cells (P = 5E-4) (Table S3). Besides, the GO term 'ER overload response (GO:0006983)' was found to be significantly enriched (P = 4.19E-02) only in the differentiated Caco-2 cells, endowing an explicit role to HNF4α in UPR during differentiation. XBP1 was also of particular interest to us as it is activated upon disruption of homeostasis in the ER and activation of the UPR [5].

We next examined the expression of XBP1 in the course of differentiation of Caco-2 cells and found an increase in the levels of both unspliced and spliced *XBP1* at both mRNA (lower panels) and protein levels (Fig. 3B). To understand whether the expression of *XBP1* was altered in tumor cells based on their degree of differentiation, we also analyzed a publicly available microarray dataset (GSE17538) that stratified tumors according to well-, moderate, and poorly differentiated tumors [33]. Interestingly, we observed that the mRNA expression of *XBP1* was higher in the well-differentiated tumors compared to the moderate differentiated tumors (moderately differentiated vs well-differentiated P = 0.004233, other comparisons were statistically not significant) (Fig. 3C). This suggested that poorly differentiated high-grade tumors, similar to undifferentiated Caco-2 cells, showed reduced levels of HNF4α (Fig. 2E) as well as reduced levels of *XBP1* mRNA further suggesting an HNF4α-mediated regulation of *XBP1* expression.

We analyzed ChIP-Seq data (publicly available GSE23436 dataset, [32]) to determine the HNF4α binding regions (peaks) in the 2000 bp upstream region of *XBP1* gene in proliferating and differentiated Caco-2 cells. We observed an enrichment in the binding of HNF4α to the *XBP1* promoter in the differentiated Caco-2 cells compared to the proliferating Caco-2 cells (Fig. 3D). To experimentally confirm whether *XBP1* was a direct target of HNF4α in differentiated Caco-2 cells, ChIP was carried out, which indicated significantly higher binding of HNF4α to the *XBP1* promoter in the differentiated compared to the undifferentiated Caco-2 cells (Fig. 3E, upper panel). Enhanced binding of HNF4α to the *CDX2* promoter in the differentiated Caco-2 cells served as a positive control in ChIP experiments (Fig. 3E, lower panel). We next analyzed a publicly available microarray dataset (GSE11759 [34]) for the expression of *Xbp1* in wild-type and conditional intestinal epithelial *Hnf4α* knockout mouse samples and found a robust and significant downregulation of *Xbp1* expression in the

Fig. 2. Enhanced expression of HNF4α in differentiated colon epithelial cells: (A) Nuclear levels of HNF4α and CDX were increased during spontaneous differentiation of Caco-2 cells (representative image from three biological replicates). (B) HNF4α expression increased in the total protein extract of differentiated Caco-2 cells (upper western blot panel). HepG2 (human hepatocellular liver carcinoma) whole cell lysate was used as a positive control. Different HNF4α antibody clones (C-19 and K9218) showed enhanced expression of HNF4α in the total extract of differentiated Caco-2 cells (lower western blot panel). Change in the protein levels of HNF4α during the course of differentiation is shown as a bar graph (on the right; n = 3). The results are given as mean ± SEM. *t*-Test was used to compare undifferentiated (subconfluent) cells with confluent (d0) or differentiated cells (d10 and d20) (ns = not significant; ****$P \leq 0.0001$). (C) *HNF4α* mRNA increased in d10 and d20 differentiated cells (left panel; n = 4), and both P1 and P2 transcripts of *HNF4α* were found to be enhanced in those cells (right panel). The results are shown as mean ± SEM (n = 4; each with three technical replicates). *t*-Test was used for comparison of undifferentiated (subconfluent) cells with day 10 or 20 differentiated cells (ns = not significant; *$P \leq 0.05$, **$P \leq 0.01$, ***$P \leq 0.001$). (D) Dataset (GSE84742) analysis from murine cells revealed higher expression of *Hnf4α* in the luminal surface (differentiated) cells (n = 4) compared to the distal colon crypt base (undifferentiated) cells (n = 4). (E) Representative images of immunostains in normal colon mucosa and CRC carcinomas that were grouped into two major classes: poorly differentiated (high-grade; grades 3 and 4, n = 173) and well-differentiated (low-grade; grades 1 and 2, n = 23). In the tumor samples, a significant association was observed between the degree of differentiation and the expression of both HNF4α and CDX2. (F) 5-mC ChIP-Sequencing data were obtained from a publicly available dataset GSE69333: GSM1697907 for day 0, GSM1697908 for day 4, GSM1697909 for day 12, and GSM16979010 for day 15. *HNF4α* gene and its isoforms are shown. Compared to day 0 undifferentiated cells, substantial increase in hydroxymethylation in the 5.0 kb upstream and 5.0 kb downstream regions of the TSS of P1 and P2 transcripts, as well as in the intragenic region of the gene, was found in the differentiated cells.

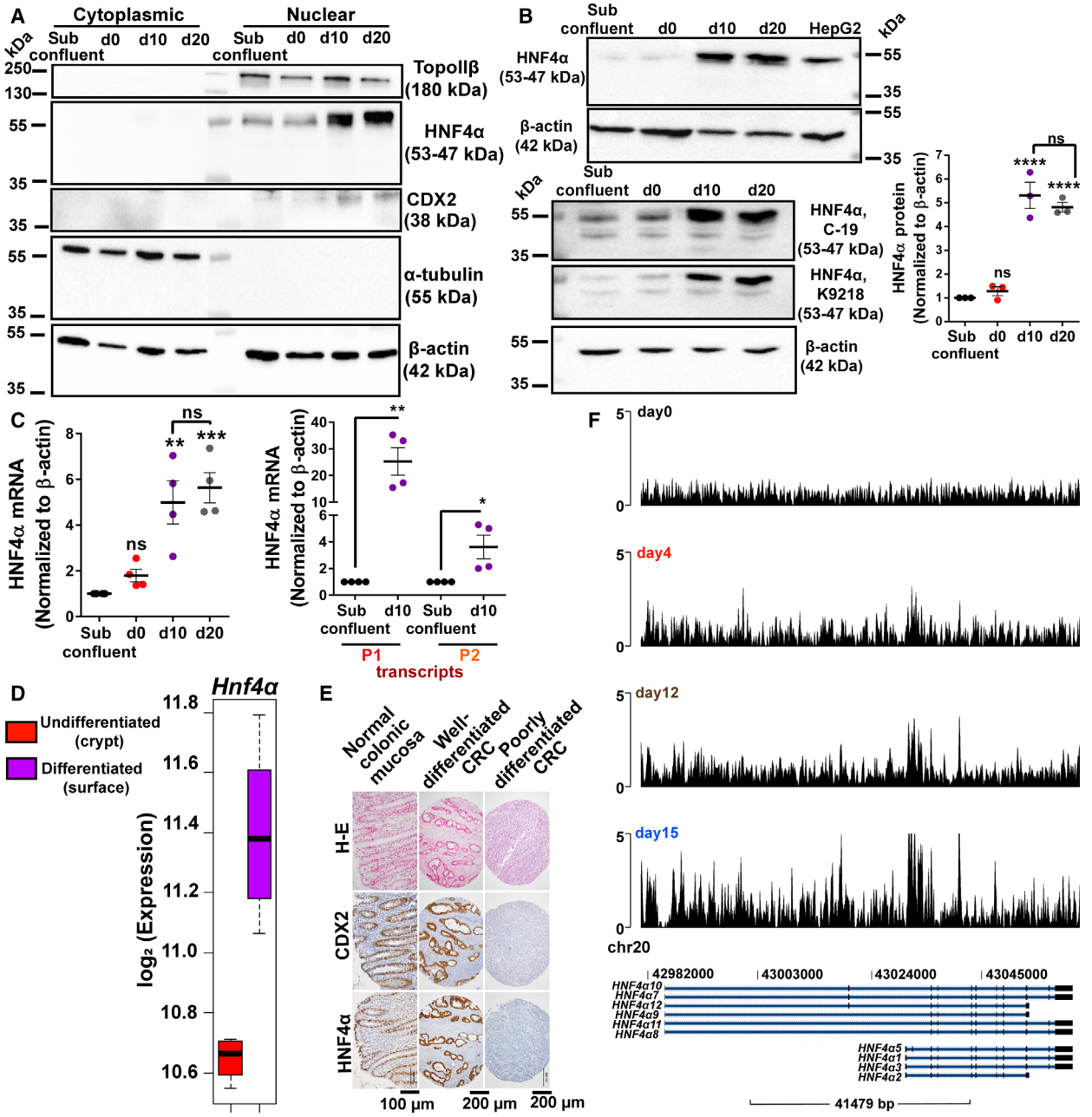

intestine of *Hnf4α* knockout mice compared with their wild-type (control) counterparts (Fig. 3F).

To determine whether ER stress induced in the course of differentiation was responsible for the increase in the expression of HNF4α, we treated undifferentiated Caco-2 cells with tunicamycin (TN), an ER stress-inducing agent. Induction of ER stress with TN was confirmed by an increase in the level of spliced *XBP1* (Fig. 3G, right panel); however, we did not observe any increase in the expression of HNF4α in the treated cells (Fig. 3G, upper panel). This suggests that ER stress occurred downstream of HNF4α activation during the differentiation of Caco-2 cells.

Activation of the endonuclease IRE1 leads to the splicing of *XBP1* mRNA. We therefore analyzed whether enhanced expression of *XBP1* in the differentiated Caco-2 cells was also accompanied by enhanced splicing [5,6]. A robust increase in phosphorylation of IRE1α at Ser724 (Fig. 4A) in concert with the increased spliced *XBP1* levels (Fig. 3B) was seen in 10 and 20 days

postconfluent Caco-2 cells. Additionally, the inhibitory phosphorylation of eIF2α at Ser51 was increased in differentiating Caco-2 cells (days 5 and 10 after reaching 100% confluency) and then decreased in the fully differentiated cells (day 20 after reaching 100% confluency) (Fig. 4B) indicating that at the early stages, the cells undergo UPR, which may be relieved at the later stages of differentiation. The results indicate that both IRE1/XBP1 and PERK/eIF2α axes were activated in Caco-2 cells during spontaneous differentiation.

Alterations in Ca^{2+} release from the ER and downstream signaling are frequently observed during ER stress [35]. We observed that intracellular Ca^{2+} level was significantly higher in day 10 differentiated Caco-2 cells compared to the day 0 cells (Fig. 4C). Intracellular Ca^{2+} can activate calmodulin-dependent protein kinase kinase beta, which in turn, is known to phosphorylate AMP-activated protein kinase (AMPK) [36]. Additionally, active AMPK can inhibit the energy sensor protein mammalian target of rapamycin (mTOR) [37]. We observed an increase in the phosphorylation of AMPK at Thr172 (Fig. 4D) as well as a reduction in the levels of p-mTOR in the differentiated Caco-2 cells, compared to the undifferentiated cells (Fig. 4E), suggesting that alterations in Ca^{2+} responsive proteins occurred due to the changes in cytosolic Ca^{2+} levels. Additionally, when we treated the undifferentiated Caco-2 cells (with lower levels of cytoplasmic Ca^{2+}) with thapsigargin (TG), a sarco/endoplasmic reticulum Ca^{2+} ATPase (SERCA) inhibitor that raises the cytoplasmic Ca^{2+} levels, we observed enhanced phosphorylation of eIF2α. Moreover, when we treated the day 10 differentiated cells (which showed enhanced ER stress and Ca^{2+} levels) with GSK2656157, a PERK inhibitor, we observed a dramatic decrease in the phosphorylation of eIF2α, while BAPTA-AM, an intracellular Ca^{2+} chelator, modestly reduced the phosphorylation of eIF2α (Fig. 4F), indicating that increase in the intracellular Ca^{2+} was not the only event responsible for the induction of UPR during differentiation.

Next, we asked whether ATF6, another transcriptional arm of UPR, is also modulated during the differentiation of Caco-2 cells. Activation of the ATF6 arm is characterized by a proteolytic cleavage of the 90 kDa full-length proform of ATF6 into an N-terminal 50 kDa (ATF6-p50) and a 36 kDa fragment (ATF6-p36) [38]. We observed an increase in the mRNA level (Fig. 5A), as well as protein expression and processing of ATF6 in differentiated Caco-2 cells (Fig. 5B). The underglycosylated form of ATF6, p90-ATF6, was detected in differentiated cells which indicates the activation of ATF6 to trigger UPR [39,40]. Additionally, analysis of the HNF4α ChIP-Seq dataset (GSE23436) indicated that the *ATF6* promoter showed enhanced HNF4α recruitment in differentiated Caco-2 cells compared to undifferentiated cells (Fig. 5C) which we

Fig. 3. HNF4α transcriptionally upregulated *XBP1* during intestinal epithelial differentiation: (A) Analysis of ChIP-Seq dataset (GSE23436) revealed statistically significant enrichment of the GO terms 'cell differentiation', 'response to ER stress', and 'autophagy' in the HNF4α binding sequences in the proliferating (undifferentiated) and spontaneously differentiated Caco-2 cells. Venn diagrams are used to represent overlapping genes for the three GO terms. *XBP1* was one of the two genes that was common to all three GO terms in the differentiated cells. (B) Western blot analysis indicated enhanced expressions of both spliced *XBP1* (*XBP1s*) and unspliced *XBP1* (*XBP1u*) in spontaneously differentiating Caco-2 cells (upper panel). qRT-PCR showed increased expression of *XBP1* mRNA, as well as splicing of *XBP1* (*XBP1s*) during spontaneous differentiation of Caco-2 cells (lower panels). qRT-PCR results are given as mean ± SEM. Statistical analyses were carried out with respect to subconfluent cells, by using *t*-Test ($n = 3$ with three technical replicates each; $^{**}P \leq 0.01$, $^{***}P \leq 0.001$). (C) Analysis of GSE17538 microarray dataset which stratified colon tumors as well, moderately, and poorly differentiated indicated higher mRNA expression of *XBP1* in the well-differentiated tumors ($n = 16$) compared to the moderate ($n = 163$) or poorly differentiated ($n = 28$) tumors. (D) Schematic representation of ChIP-Seq (GSE23436 dataset) peaks in the 2000 bp upstream region of *XBP1* gene in proliferating (GSM575228) and differentiated (GSM575229) Caco-2 cells. *XBP1* gene and its 2000 bp upstream region are shown. 2.42 fold enrichment ($P = 0.51E\text{-}3$) in the binding of HNF4α at the *XBP1* promoter (region between the bases 27526717-27526996, on chr22) was found in the differentiated Caco-2 cells with respect to undifferentiated (subconfluent) cells. ChIP-Seq data from three pooled experiments were analyzed. (E) ChIP assay revealed that HNF4α binding site enrichment in the *XBP1* promoter (chrbiop22; between the bases 27526796 and 27526967) was higher in the differentiated Caco-2 cells with respect to proliferating (subconfluent) cells (upper panel) ($n = 5$; each with three technical replicates). HNF4α binding at the *CDX2* promoter used as a positive control (lower panel) ($n = 4$; each with three technical replicates). ChIP data obtained by qRT-PCR for the HNF4α antibody were normalized to IgG controls and plotted as fold change (mean ± SEM). *t*-Test was used to compare enrichment of the HNF4α binding at the *XBP1* or *CDX2* promoters in subconfluent (undifferentiated) and 10-day differentiated cells ($^{*}P \leq 0.05$, $^{**}P \leq 0.01$). (F) Probe-specific expression of *Xbp1* was analyzed in wild-type and *Hnf4α* knockout (mutant) samples (GSE11759). For probe 1 (1420011_s_at), $P = 0.004951825$; for probe 2 (1420012_at), $P = 0.322953318$; for probe 3 (1420886_a_at), $P = 0.007230887$; for probe 4 (1437223_s_at), $P = 0.00466318$). (G) qRT-PCR showed that the levels of spliced *XBP1* (*XBP1s*) increased with TN treatment in subconfluent Caco-2 cells (on the right), but did not affect the level of HNF4α expression in undifferentiated Caco-2 cells (on the left). For qRT-PCR, results are shown as mean ± SEM ($n = 3$; each with three technical replicates) and *t*-test was used to compare veh. (DMSO)-treated Caco-2 cells with TN-treated Caco-2 cells ($^{****}P \leq 0.0001$).

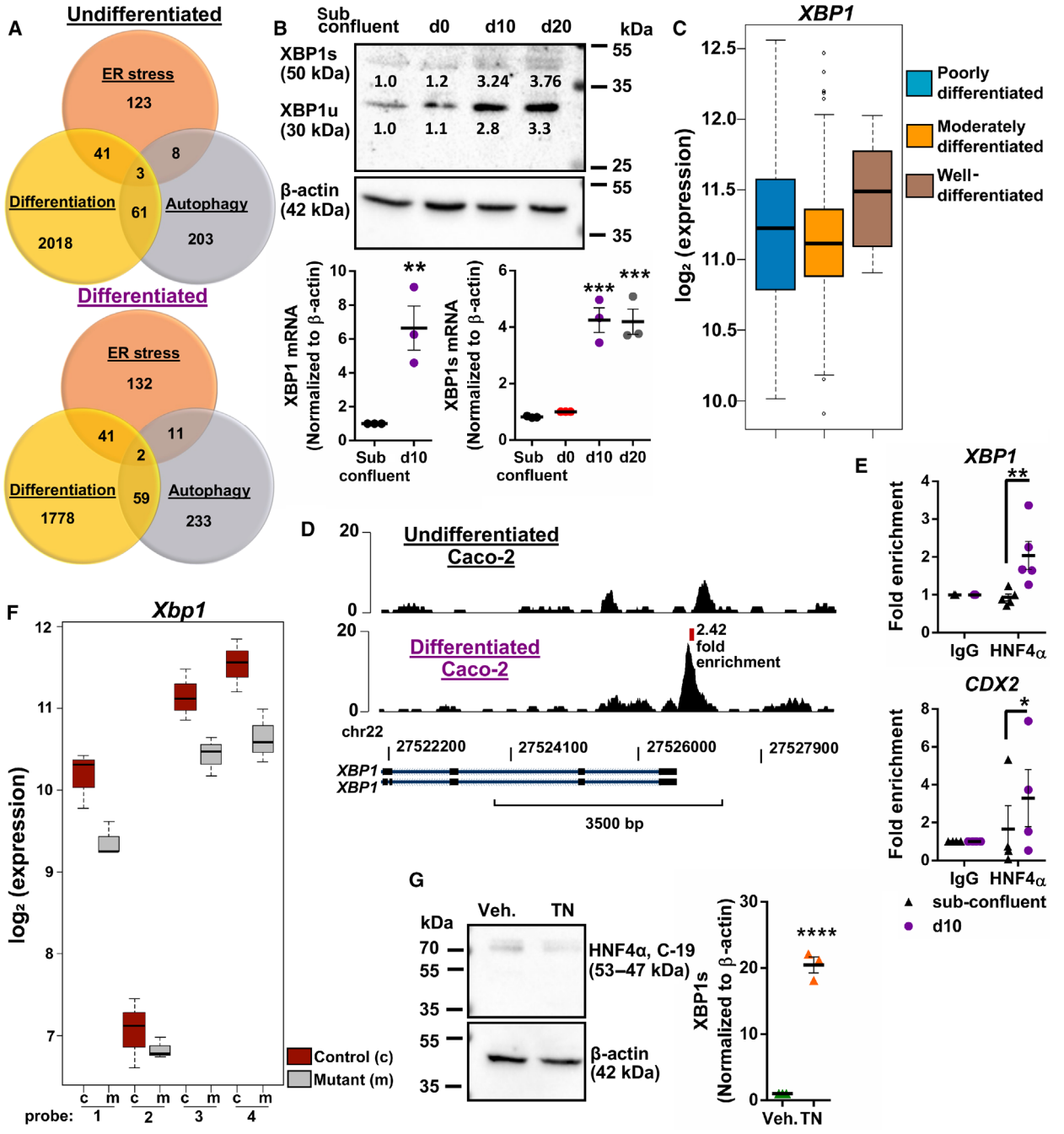

further confirmed experimentally by ChIP (Fig. 5D). Similar to the expression of *HNF4α* and *XBP1*, *in silico* analysis of the expression of *ATF6* (GSE17538) was found to be related to the extent of differentiation of colon tumors; thus, lower expression was seen in poorly differentiated cancer samples compared to moderate and well-differentiated samples (poorly differentiated vs well-differentiated $P = 0.036023$, other comparisons were statistically nonsignificant) (Fig. 5E).

Interaction of HNF4α with the promoters of two well-known ER stress markers, XBP1 and ATF6, prompted us to ask the extent to which HNF4α regulates gene expression during UPR. Analysis of GSE11759 microarray data indicated that 23% of genes under the GO term 'Response to ER Stress' (GO:0034976) [35] was differentially expressed in intestinal epithelial cells between wild-type and *Hnf4α* knockout mouse ($P < 0.05$) (Fig. 5F).

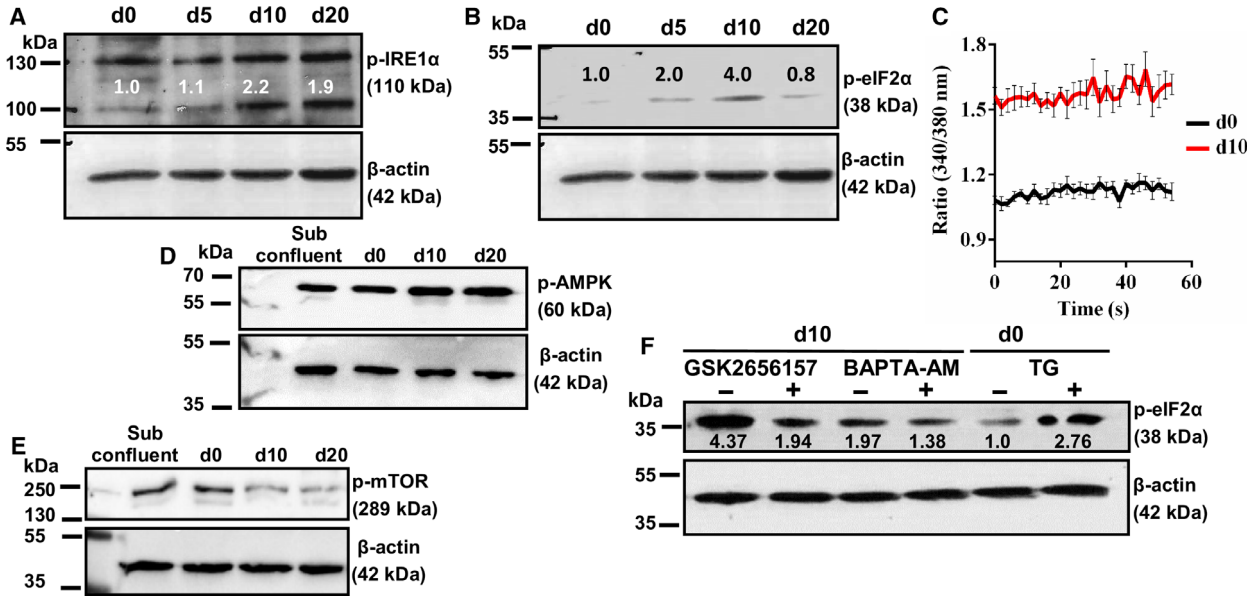

Fig. 4. Intracellular level of Ca^{+2} increased and IRE1 and PERK; arms of UPR, were induced in Caco-2 cells undergoing differentiation: (A) Increased IRE1α and (B) eIF2α phosphorylation were seen in differentiating Caco-2 cells indicating the activation of ER stress pathways (representative western blot of two biological replicates). (C) Cytoplasmic level of Ca^{+2} was increased in day 10 postconfluent Caco-2 cells (n = 5). (D) Western blot showed an increase in the phosphorylation of AMPK (representative immunoblot of three biological replicates) (E) and a decrease in phosphorylation of mTOR during the differentiation of Caco-2 cells (representative of two biological replicates). (E) Phosphorylation of eIF2α at Ser51 in the differentiated Caco-2 (d10) cells could be reversed with the PERK inhibitor GSK2656157 and induced in the undifferentiated cells (d0) with the SERCA inhibitor TG. (F) A very modest reduction in the phosphorylation of eIF2α was observed in differentiated Caco-2 cells treated with BAPTA-AM, an intracellular Ca^{2+} chelator (representative western blot of two biological replicates).

ER stress leads to the induction of autophagy in differentiating epithelial cells

Activation of ER stress is very frequently accompanied by the development of autophagy [11]. We asked whether the induction of differentiation in Caco-2 cells could induce autophagy in these cells. We observed an enhanced ratio of LC3-II/LC3-I, increased levels of Beclin-1 protein, and reduced levels of p62 protein (indicating enhanced autophagic flux) (Fig. 6A) as well as increased content of autophagy vesicles during spontaneous differentiation model of Caco-2 cells (Fig. 6B, C). Increased LC3 puncta formation in the differentiated Caco-2 cells when compared to the undifferentiated cells was also observed (Fig. 6D). Additionally, both ER stress and autophagy have been implicated in the process of differentiation [4,41]. Examination of the GO term 'Autophagy' (GO:0006914) indicated that 24% genes were statistically significantly differentially expressed between *Hnf4α* wild-type and *Hnf4α*

Fig. 5. ATF6 is transcriptionally regulated by HNF4α and activated during differentiation: (A) qRT-PCR shows that mRNA expression of *ATF6* increases during the course of differentiation (n = 4; each with three technical replicates). The results (mean ± SEM) were analyzed with respect to subconfluent cells by using t-Test (**$P \leq 0.01$). (B) Western blot showing an increase in the levels of cleaved ATF6 in spontaneously differentiating Caco-2 cells. The levels of unprocessed ATF6 were observed to decrease in the differentiated cells (representative of two biological replicates). (C) Schematic representation of ChIP-Seq (GSE23436 dataset) peaks in the 2000 bp upstream region of *ATF6* gene in proliferating (GSM575228) and differentiated (GSM575229) Caco-2 cells. In the lower panel, HNF4α binding site enrichment regions ($P < 0.05$) in the *ATF6* promoter in differentiated Caco-2 cells with respect to proliferating (subconfluent) Caco-2 cells are given as bar plots (GSE23436). ChIP-Seq data from three pooled experiments were analyzed. (D) ChIP assays show that HNF4α binding site enrichment in *ATF6* promoter (chr1; between the bases 161766125 and 161766363) was higher in the differentiated Caco-2 cells with respect to proliferating (subconfluent) cells. ChIP qRT-PCR results (n = 3, with three technical replicates for each; mean ± SEM) were normalized to IgG controls and given as fold change. t-Test was used to compare enrichment of HNF4α binding at the *ATF6* promoter in undifferentiated (subconfluent) and differentiated (d10) cells (***$P \leq 0.001$). (E) Analysis of GSE17538 microarray dataset indicates higher mRNA expression of *ATF6* in the well-differentiated tumors (n = 16) compared to the moderate (n = 163) or poorly differentiated tumors (n = 28). (F) Pie chart shows 19 out of 82 ER stress-related genes (GSE11759 dataset) were differentially expressed in *Hnf4α* knockout mice (n = 3) compared to wild-type controls (n = 3). Selection criteria were based on $P < 0.05$.

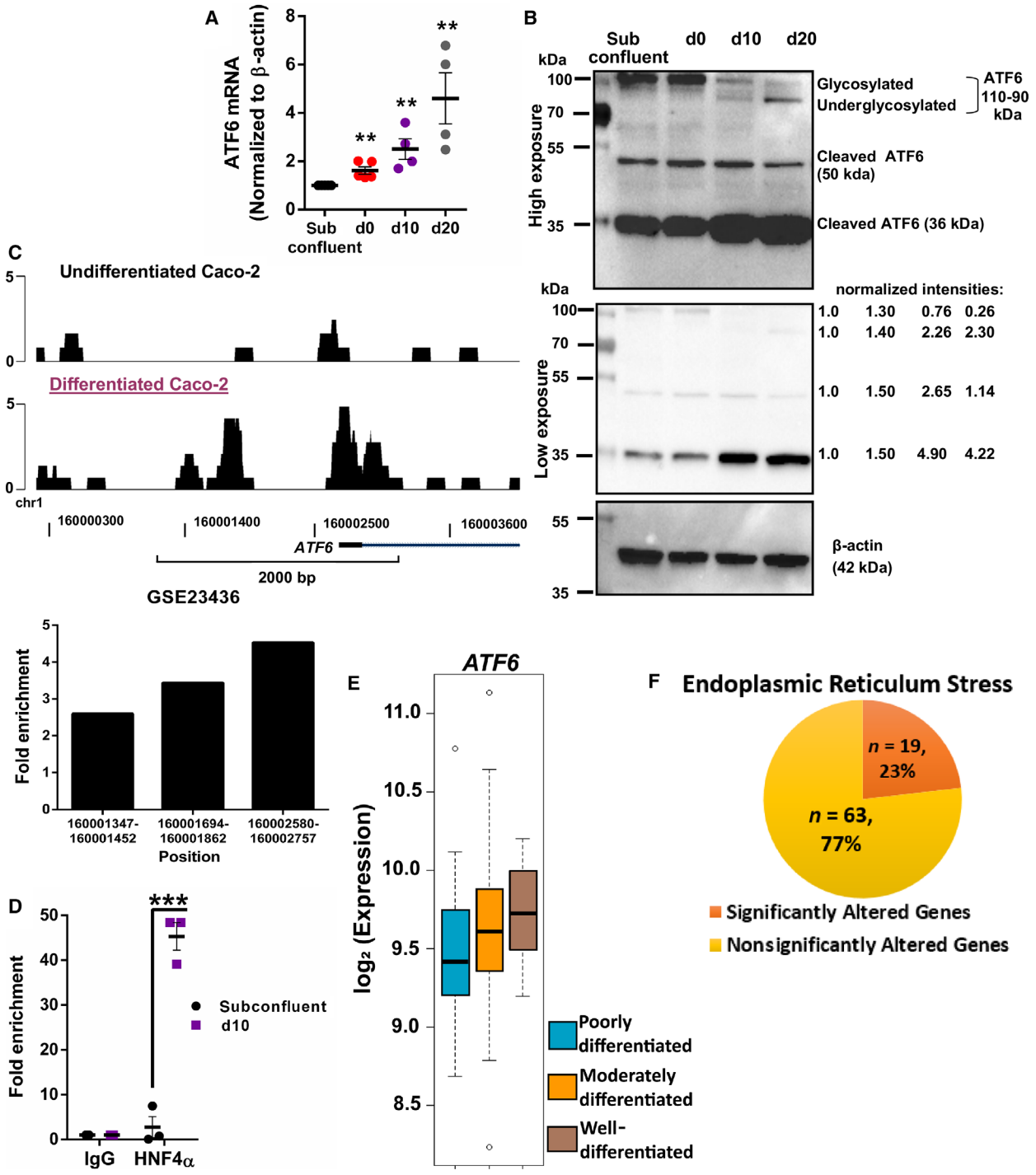

knockout mice (GSE11759) (Fig. 6E). This result suggests that the HNF4α-regulated ER stress observed in differentiating Caco-2 cells may also lead to the induction of autophagy.

Since the Caco-2 model of differentiation requires the cells to be confluent, we queried whether the increase in expression of HNF4α and observed autophagy in the differentiated cells could simply be attributed to cell confluency. We examined the expression of HNF4α in the colon cancer cell line SW-480 that was cultured for 10 days after reaching 100% confluency. These cells showed the confluency-dependent increase in the expression of CEA but did not show an increase in the expression of HNF4α (Fig. 7A). Importantly, we observed an

Fig. 6. Induction of autophagy in differentiating colon epithelial cells: (A) Expression of three ATG proteins, LC3, Beclin-1, and p62, is shown by western blot (representative immunoblot of three biological replicates). Ratio of LC3-II to LC3-I, as well as Beclin-1 expression increased, while p62 protein level decreased in differentiated Caco-2 cells. *t*-Test was used to compare LC3-II to LC3-I ratio (n = 10; mean ± SEM) in subconfluent cells with confluent (d0) or differentiated (d10 and d20) cells (**$P \leq 0.01$, ***$P \leq 0.001$). (B) Formation of autophagic vacuoles in differentiated Caco-2 cells. Rapamycin (Rap)- and chloroquine (CHQ)-treated subconfluent Caco-2 cells were used as positive control. Subconfluent cells, confluent-undifferentiated cells (d0), and 10-day differentiated cells (d10) were stained with CYTO-ID® Green Detection Reagent and analyzed by flow cytometry. Results are presented as a histogram overlay. Subconfluent cells were used for gating (M1), and unstained cells were used to determine the level of background fluorescence. Increased percentages of Cyto-ID®-positive cell populations (M1%) and enhanced magnitude of fluorescence signal (mean fluorescence intensity) were observed in the differentiated cells (n = 2). The results (mean ± SEM) were analyzed with respect to subconfluent cells by using *t*-Test (*$P \leq 0.05$, **$P \leq 0.01$). (C) Fluorescent puncta inside the Caco-2 cells represent Cyto-ID® Green autophagy dye-stained autophagosomes/autolysosomes. Autophagy induction in differentiated Caco-2 cells was quantified by the determination of mean fluorescence intensities. Scale bars show 11 μm. The results of four biological replicates are given as mean ± SEM. *t*-Test was used for comparing subconfluent cells with the other experimental groups (**$P \leq 0.01$, ***$P \leq 0.001$). (D) Undifferentiated and differentiated Caco-2 cells were transiently transfected with the GFP-LC3 plasmid for puncta quantification. The number of cells containing GFP-LC3 punctate increased significantly on day 10 compared to day 0 Caco-2 cells. The result belongs to four biological replicates and is shown as mean ± SEM. *t*-Test was used for comparison (****$P \leq 0.0001$). (E) Pie chart shows 23 out of 95 ATG genes were differentially expressed when *Hnf4α* was knocked down (GSE11759 dataset). The genes were selected according to $P < 0.05$.

increase in the ratio of LC3-II/LC3-I in differentiated T84 colon cancer cells that can also undergo contact-dependent spontaneous differentiation compared to undifferentiated subconfluent cells (Fig. 7B). Therefore, it can be concluded that enhanced HNF4α expression and observed autophagy in the spontaneously differentiated Caco-2 cells are differentiation-dependent, rather than confluency-dependent.

Discussion

Caco-2 cells are derived from a colon adenocarcinoma, but have the ability to differentiate into enterocyte type cells and are considered to be a good model for the differentiation of committed gut epithelial cells [42]. HNF4α is a transcription factor that is known to be highly enriched in promoters of genes upregulated in the crypt to villus axis and orchestrates key processes such as intestinal epithelial cell differentiation, nutrient metabolism, barrier functions, and protection against pathogens [3,35]. Increased activity of HNF4α in the differentiated cells is accompanied by its increased expression. We suggest that this increased expression could have resulted from increased hydroxymethylation of cytosines in the promoter and coding region of HNF4α in the differentiated cells. The covalent modification of cytosine (C) to 5-methylcystosine (5mC) is an important regulator of gene expression [43]. 5mC can be enzymatically converted to 5-hydroxymethylcytosine (5hmC) through the activity of TET. Analyses of genomic 5mC and 5hmC sequences demonstrate depletion or enrichment of these modified cytosine residues in mammalian promoters, exons, gene bodies, enhancers, and gene clusters [44]. 5hmC is generally enriched about 0.5–2 kb upstream and downstream of the TSS, and there is a positive correlation between the level of gene expression and enrichment for 5hmC in the body of genes [30,44] suggesting that hydroxymethylation observed in both the promoter and coding region of HNF4α could have contributed to the increase in expression observed.

We observed for the first time that the increase in expression and activity of HNF4α during differentiation led to the transcriptional upregulation of two of the three primary ER stress mediators: XBP1 and ATF6. HNF4α, which is considered to be important in the development of endodermal organs, is also required for continued maintenance of XBP1 in differentiated, adult cells [9,10]. Analysis of a publicly available ChIP-Sequencing dataset (GSE23436) [32] indicated that the only gene that showed promoter enrichment for HNF4α in the differentiated Caco-2 cells that was common to the GO terms ER stress, cell differentiation, and autophagy (please see below for further discussions on autophagy) was *XBP1*. Besides its function as an UPR regulator, XBP1 is also recognized as a major regulator of highly secretory cells such as plasma cells, Paneth cells, pancreatic acinar cells, mammary epithelial cells, and salivary gland cells, and is selectively required for granulocyte maturation [45–47]. The levels of XBP1 and p-eIF2α were shown to be very low in crypt base columnar cells compared to the TA cells higher up in the crypt [7], revealing that ER stress and eIF2α signaling may also have roles in mediating the complex signals needed for the differentiation of intestinal epithelial stem cells. As one of the three arms of UPR, ATF6 was also found to be upregulated and activated during the spontaneous differentiation of colon epithelial cells through increased recruitment of HNF4α to the *ATF6* promoter in differentiated cells.

Proteomic analysis of spontaneously differentiated Caco-2 cells indicated that many of the significantly upregulated proteins have a function in lipid metabolism

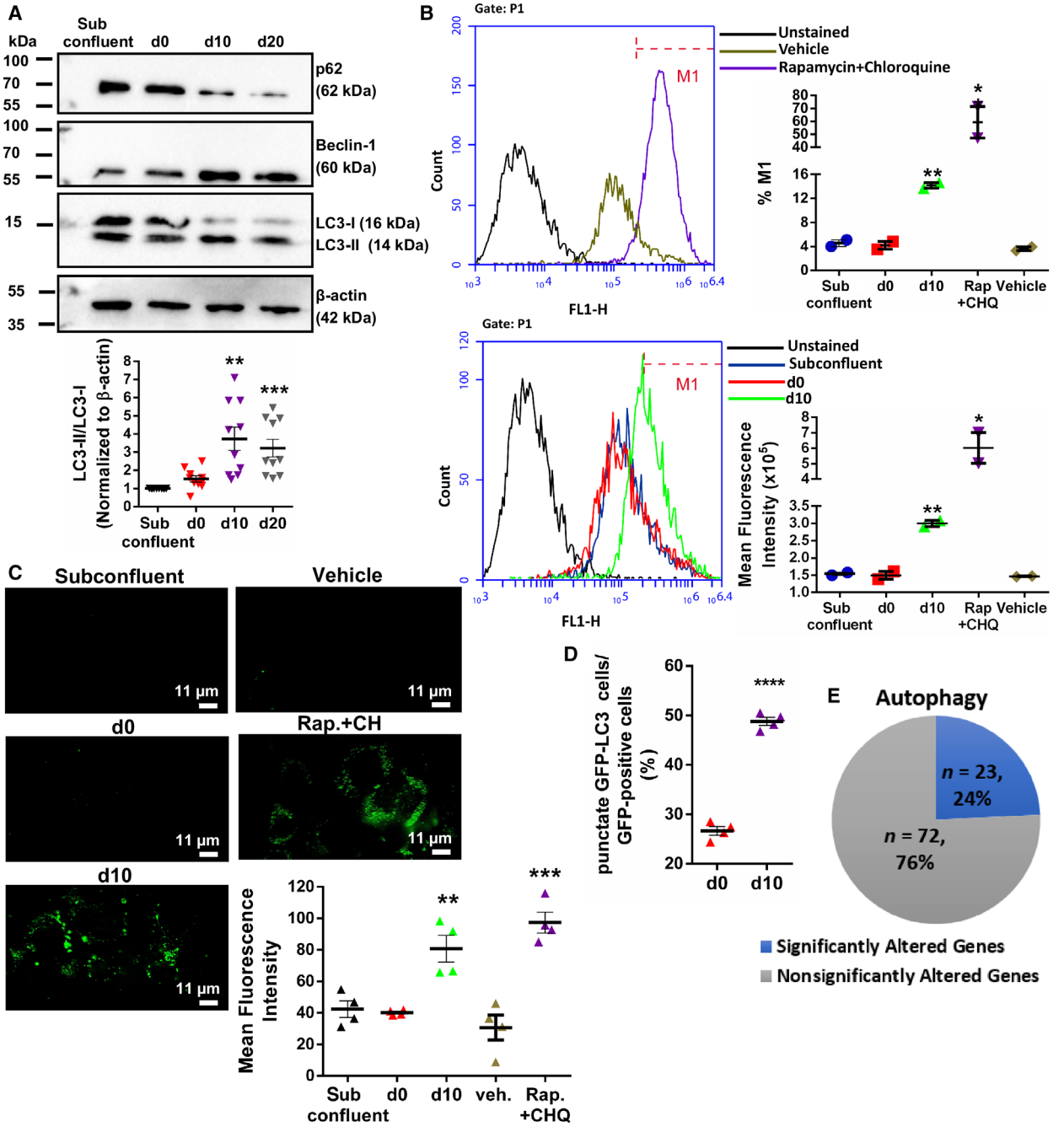

[22]. While a broad spectrum of insults such as nutrient deprivation, changes in calcium concentration, failure of post-translational modifications, or increase in secretory protein synthesis can lead to protein misfolding in the ER and activate UPR, each individual UPR pathway also has unique and specialized roles in diverse developmental and metabolic processes [48,49]. For example, the ER is a major site of lipid metabolism and many relevant enzymes are located in this organelle. Enterocytes accumulate lipids through fatty acid and cholesterol transport as well as *de novo* biosynthesis; and HNF4α, in particular, was shown to regulate the expression of genes necessary to absorb dietary lipids in enterocytes [20]. Recent findings highlight ATF6 as a major regulator of organogenesis, differentiation, and tissue homeostasis [50,51] as well as cellular metabolism [52]. Collectively, our data suggest that the HNF4α-mediated increase in the expression of XBP1 and ATF6 and induction of ER

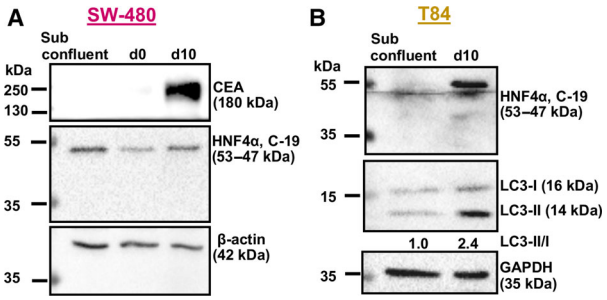

Fig. 7. HNF4α expression and autophagy depend on differentiation rather than culture confluency in the Caco-2 and T84 spontaneously differentiating models of intestinal epithelial cells. (A) Expression levels of HNF4α in SW-480 colon cancer cell line cultured under confluency for 10 days are shown by western blot (representative of two biological replicates). (B) Enhanced HNF4α expression and increase in the LC3 II/I ratio are shown by western blot in spontaneously differentiated T84 cells (representative of three biological replicates).

stress and UPR may activate a novel regulatory network module that can orchestrate lipid homeostasis and energy status during enterocyte differentiation.

ER stress is closely associated with the development of autophagy [11], primarily as a mechanism to alleviate ER stress. Our data indicate that even in nutrient replete conditions, autophagy was induced during spontaneous differentiation along with the activation of the AMPK-mTOR signaling cascade, most likely due to increased cytosolic Ca^{2+} levels. Additionally, increased cytosolic Ca^{2+} can activate the kinase death-associated protein kinase-1 (DAPK1), which in turn, can favor the release of Beclin-1 from inhibitory interactions with Bcl2 and initiate autophagy [53]. We have observed an increase in the mRNA expression of DAPK1 during the course of differentiation of Caco-2 cells (data not shown). Thus, in the current study, increased Ca^{+2} levels and subsequent signaling could have led to the induction of autophagy [54]. Several recent findings have indicated that a steady-state induction of autophagy is necessary for the maintenance of intestinal stem cells by reducing ROS and DNA damage and ensuring proper cell cycle progression [55,56]. Autophagy also plays a crucial role as a cellular stress responder by providing alternative energy source following starvation or by degradation of intracellular components and can function in different cellular contexts such as cell differentiation and cell-fate determination, adult stem cell self-renewal, somatic cell reprogramming, organogenesis, and mitigation of inflammation [57–59]. A recent study conferred a novel role for autophagy in the gut. The authors showed that ER stress protected against decreased barrier function and ER stress-mediated ATF6/DAPK1 signaling in enterocytes led to enhanced autophagy-mediated killing of bacteria (xenophagy) thereby reducing the potential for metabolic stress to reactivate or maintain inflammation [60]. Therefore, it is likely that both enhanced biosynthesis of macromolecules, changes in metabolism, and altered Ca^{2+} homeostasis in the differentiated cells may have led to ER stress and subsequently to the induction of autophagy.

Overall, we attribute a novel function to HNF4α as a mediator of UPR resulting from ER stress during colon epithelial differentiation through the transcriptional upregulation of *XBP1* and *ATF6* during enterocyte differentiation (Fig. 8). Recently, Lambert *et al.*[61] have shown that all HNF4α isoforms have diverse functions in colon cancer cell line models and Ko *et al.*[26] have demonstrated that each isoform heterodimer and isoform homodimer pair can regulate distinct subsets of genes in an *in vitro* model of human hepatocytes. This suggests that differential expression of the various HNF4α isoforms as well as their association as hetero- and/or homodimers may determine the expression profile of HNF4α target genes in a given

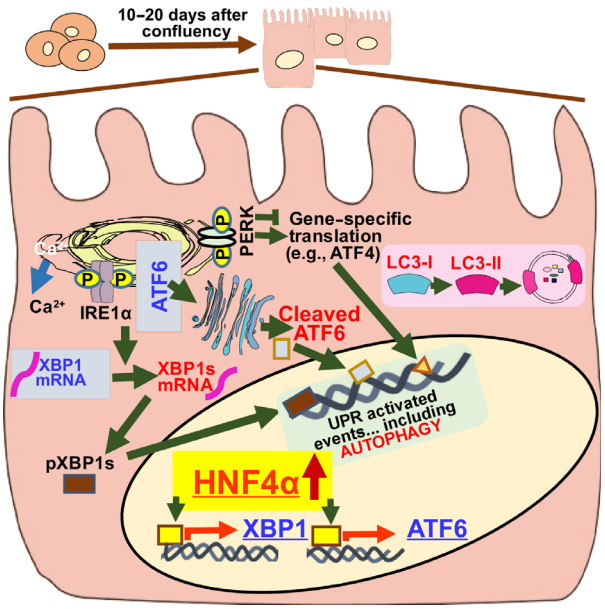

Fig. 8. Increased expression of HNF4α in differentiating colon epithelial cells orchestrates an ER stress response. ER stress activates UPR by three sensors located at the ER membrane: IRE1α, ATF6, and PERK. We have shown that with a concomitant increase in the cytoplasmic calcium (Ca^{2+}) levels, all three arms of UPR are activated in the Caco-2 model of epithelial differentiation. HNF4α functions as a key mediator of UPR through the transcriptional upregulation of *XBP1* and *ATF6*. Additionally, as a downstream UPR event, autophagy was also seen to be activated during differentiation.

tissue. Since both P1 and P2 isoforms were shown to be upregulated during the course of differentiation, with a stronger increase in the P1 transcripts, future studies on the expression and dimerization patterns of individual HNF4α isoforms can help clarify the mechanism by which HNF4α regulates target gene expression, particularly during epithelial differentiation.

Materials and methods

Cell culture, differentiation, and treatments

Caco-2 cells (ŞAP Enstitüsü, Ankara, Turkey) were grown in Eagle's minimum essential medium (Thermo Fisher Scientific, Boston, MA, USA) containing 20% FBS, 2 mM L-glutamine, 1× nonessential amino acids, 1% penicillin–streptomycin, and 1 mM Na pyruvate at 37 °C in a humidified atmosphere of 5% CO_2 and 95% air. For the induction of differentiation [62], cells were grown to confluency (day 0), after which the cells were collected at various intervals.

Treatments of Caco-2 cells were carried out at 37° C as follows: Cells were treated with 1 μM TG for 6 h; 25 μM of the intracellular Ca^{2+} chelator BAPTA-AM for 6 h in Ca^{2+} free medium; 1 μM of the PERK inhibitor GSK2656157 for 1 h; and 5 $\mu g \cdot mL^{-1}$ TN for 24 h. DMSO was used as vehicle (annotated as veh. in figures) for GSK2656157, TG, and TN treatments.

T84 cells (ATCC) were grown in 1 : 1 mixture of Ham's F12 medium (Gibco, Waltham, MA, USA) and Dulbecco's modified Eagle's medium (Gibco) with 10% FBS, 2 mM L-glutamine, and 1% penicillin–streptomycin at 37 °C in a humidified 5% CO_2 incubator. The cells were differentiated spontaneously as described for the Caco-2 cells.

SW-480 cells were obtained from ATCC (Middlesex, UK) and grown in RPMI-1640 supplemented with 10% FBS, 2 mM L-glutamine, and 1% penicillin–streptomycin at 37 °C in a humidified 5% CO_2 incubator. Cell culture medium and supplements were purchased from Biological Industries, Beit Haemek, Israel.

Alkaline phosphatase activity

Alkaline phosphatase activity was determined by using p-nitrophenyl phosphate (Sigma-Aldrich, St. Louis, MO, USA) as a substrate. The substrate (200 μL) was added to 10 μL of the total protein in a 96-well plate, mixed by pipetting, and incubated at room temperature in the dark for 30 min. The absorbance of the samples was measured at 405 nm in a spectrophotometer, and the specific activity was calculated.

For a qualitative analysis of ALP activity, a nitro blue tetrazolium chloride/5-bromo-4-chloro-3-indolyl phosphate p-toluidine (NBT/BCIP) salt (Roche, Basel, Switzerland) was used. Briefly, Caco-2 cells were grown to confluency and cultured further 10 and 20 days. At each time point, the cells were washed with 1× TBS twice and fixed in 70% EtOH for 10 min followed by three washes with 1× TBS. A single NBT/BCIP tablet was dissolved in 10 mL ddH_2O immediately before use, and the cells were incubated for 2 h in the dark with this staining solution at room temperature. The reaction was stopped by washing the cells with 1× TBS. The plate was photographed using an Olympus CKX41 inverted microscope (Shinjuku, Tokyo, Japan) equipped with Olympus U-CMAD3 camera.

Tissue microarray construction and immunohistochemistry

Four TMAs were constructed from formalin-fixed paraffin-embedded tissues of CRC carcinoma (CRC) by the Advanced Tissue Arrayer (ATA100; Chemicon, Temecula, CA, USA) manual arrayer. From 202 CRC cases, one or two 1-mm spots of representative tumor tissues (adenocarcinoma $n = 193$, adenosquamous carcinoma $n = 1$, malignant epithelial tumor $n = 1$, medullary carcinoma $n = 1$, mucinous carcinoma $n = 5$, synchronous adenocarcinoma $n = 2$) and normal colon mucosa samples ($n = 14$) were included in these TMAs. The TMAs containing human colon tissue and cancer samples were constructed with the approval from the Non-Interventional Clinical Research Ethics Committee of Hacettepe University (HEK 12/147-22). In this process, informed consent from patients was obtained.

Four-micrometer-thick sections were stained with hematoxylin–eosin for histologic assessment of the samples in the TMAs. After the confirmation of diagnosis, additional sections were immunohistochemically stained for HNF-4α using a polyclonal goat antibody (1 : 100 dilution). For this, the slides were first deparafinized by incubation at 75 °C for 40 min followed by two washes with xylene for 10 min each followed by rehydration in decreasing concentrations of ethyl alcohol (96%, 90%, and 70%, respectively). Antigen retrieval was carried out by heating the slides for 10 min in citrate buffer at pH 6.0 (Genemed Biotechnologies Inc. San Francisco, CA, USA) in a microwave. After that, samples were blocked using biotinylated rabbit anti-goat secondary antibody (BA-5000; Vector Laboratories, Burlingame, CA, USA), and the avidin-biotin peroxidase method was carried out. The signals were developed using the 3,3′-diaminobenzidine (DAB, TA-125-HD; Thermo Scientific/LabVision, Waltham MA, USA) as a chromogen. Finally, samples were stained with hematoxylin briefly for counterstaining. Dehydration and preparation of slides for microscopic examination were performed as required. Immunostaining for p53, CDX2, and CTSE was carried out in a similar manner. The primary and the antigen retrieval methods are shown in Table S4. UltraVision Polyvalent (Rabbit-Mouse) HRP Kit (TP-125-HL; Thermo Scientific/LabVision) was used for the secondary antibody and the avidin-biotin peroxidase method. All immunostains were developed using DAB.

Degree of differentiation (histologic grading) was assessed by reviewing the TMA spots and assigning a differentiation score per case using the grading system recommended by the College of American Pathologists (https://documents.cap.org/protocols/cp-gilower-colonrectum-17protocol-4010.pdf accessed 5/3/2017) (1: well-differentiated, 2: moderately differentiated, 3: poorly differentiated, and 4: undifferentiated). Nuclear HNF4α staining was assessed by semiquantifying the strength of overall staining per case (0: no staining, 1: weak staining, 2: strong staining). CDX2 immunostain was assessed in a similar manner. SPSS (version 23.0, IBM, Armonk, NY, USA) was used for tabulation and statistical analysis. Pearson chi-square test was used to assess the relationship between immunohistochemical expression scores and histologic grades of tumor. The relationship between immunostaining scores themselves was assessed with Kendall rank correlation coefficient.

Protein isolation and western blot

Total cellular proteins were isolated from proliferating or confluent Caco-2 cells using the M-PER Mammalian Protein Extraction Reagent (Thermo Scientific) containing 1× protease and phosphatase inhibitors (Roche), in accordance with the manufacturer's instructions. Nuclear and cytoplasmic fractions were isolated from proliferating or confluent Caco-2 cells grown in T25 flasks. At specific days after reaching confluency, the cells were washed with ice-cold PBS twice followed by incubation in a hypotonic buffer (300 μL, on ice for 15 min) containing 10 mM HEPES pH 7.5, 4 mM NaF, 10 μM Na2MoO4, 0.1 mM EDTA, 1× Protease and phosphatase inhibitors (Roche). After this, the samples were transferred to Eppendorf tubes and mixed with 75 μL of 10% NP40 (Pan-Reac AppliChem, Darmstadt, Germany) by gentle pipetting followed by centrifugation for 30 s at 4 °C at 14 000 ***g***. The supernatants were collected in prechilled Eppendorf tubes as the 'cytoplasmic fractions'. The nuclear pellet remaining in the tube was resuspended in 80 μL of a nuclear extraction buffer containing 10 mM HEPES, pH 7.9, 1 mM DTT, 0.1 mM EDTA, 420 mM NaCl, 1.5 mM $MgCl_2$, 10% glycerol, 1× protease and phosphatase inhibitors. The tubes were vortexed for 15 s at the highest speed followed by incubation in an orbital shaker at 4° C for 15 min followed by another round of vortexing for 30 s at 15-min intervals. The samples were centrifuged for 10 min at 14 000 ***g***, and the supernatants were collected in prechilled Eppendorf tubes as the 'nuclear fractions'. The temperature was maintained at 4° C for every step.

For western blot, total (20–50 μg) or cytoplasmic and nuclear fractions (5–10 μg) were separated using 10% SDS/PAGE gels followed by wet-transfer to poly(vinylidene difluoride) membranes using standard techniques. For a list of antibodies used, please see Table S5. The bands were developed using a Clarity ECL Substrate (Bio-Rad, Hercules, CA, USA) and visualized in a ChemiDoc MP Imaging System (Bio-Rad). Band intensities were normalized to the housekeeping proteins β-actin or GAPDH, and the results are given as 'fold change'. TopoIIβ and α-tubulin were used as nuclear and cytoplasmic markers, respectively.

RNA isolation, cDNA synthesis, and qRT-PCR assays

Total RNA from Caco-2 cells at different days after confluency was isolated using the RNeasy RNA Extraction Kit (Qiagen, Hilden, Germany) according to the manufacturer's guidelines. The RNA was treated with DNAseI (Thermo Scientific) to remove genomic DNA contamination, and cDNA synthesis was carried out using 500 ng of the RNA using RevertAid First Strand cDNA Synthesis Kit (Thermo Scientific).

For real-time PCR (RT-qPCR), a Rotor GeneQ 6000 (Qiagen) was used. Relative expressions were calculated with respect to the housekeeping gene (β-actin) using the Pfaffl method [63], and the results were expressed as 'fold change'. All RT-qPCRs followed the MIQE guidelines [64]. Primer sequences used for expression analyses are shown in Table S6.

Intracellular calcium measurement

Caco-2 cells were grown to confluency in T25 flasks and either collected immediately (day 0) or kept growing post-confluency for 10 days (day 10 samples). At the time of collection, the cells were detached by trypsin, washed with complete medium, and centrifuged for 10 min at 14 000 ***g***. To detect intracellular Ca^{2+} Fura-2/AM (Invitrogen, Carlsbad, CA, USA), a cell permeable ratiometric fluorescent dye that can bind to free calcium was used. The cells were loaded with 2.5 μM of the dye for 45 min at 37 °C in Ca^{2+}-standard buffer containing 145 mM NaCl, 5 mM KCl, 1 mM $MgCl_2$, 1 mM $CaCl_2$, 10 mM glucose, and 10 mM HEPES (pH 7.4). The cells were then centrifuged and resuspended in Ca^{2+}-standard buffer for 15 min at room temperature for de-esterification followed by three washes in the same buffer.

To determine the Ca^{2+} levels, fluorescence was measured from 100 μL aliquots of cells (containing approximately 1×10^6 cells per mL) at 37 °C every 2 s for 60 s using a Spectramax M5 microplate reader (Molecular Devices, San Jose, CA, USA) at an excitation wavelength of 340 nm (complexed calcium) and 380 nm (free calcium) and at a fixed emission at 510 nm. To eliminate the background fluorescence, fluorescent readings from the same number of cells not loaded with Fura-2/AM were subtracted from the fluorescence values of the Fura-2/AM-loaded samples. A ratio of the 340 nm/380 nm fluorescence signals was indicative of the free cytosolic Ca^{2+} concentration.

Imaging and flow cytometry-based detection of autophagy

To detect autophagic flux in the proliferating and differentiated Caco-2 cells, a CYTO-ID® Autophagy Detection Kit (Enzo Life Sciences, Farmingdale, NY, USA) was used. Subconfluent (60–70% confluent), 100% confluent (day 0), and differentiated (day 10) cells were used for this assay as described previously [13]. As a positive control, autophagy was induced in subconfluent Caco-2 cells incubated for 24 h with 500 nM rapamycin and 30 μM chloroquine. Subconfluent Caco-2 cells incubated with vehicle (DMSO and dH_2O for rapamycin and chloroquine, respectively) under identical culture conditions were used as negative controls. To quantitatively determine autophagic flux, proliferating or differentiated Caco-2 cells were incubated with the CYTO-ID® Green Detection Reagent and assayed in the green channel (FL1) of a BD Accuri™ C6 flow cytometer (BD Biosciences, Ann Arbor, MI, USA). For a qualitative analysis of the autophagic puncta, CYTO-ID®-stained autophagosomes/autolysosomes in proliferating or differentiated Caco-2 cells were examined under a Leica DMI4000 confocal microscope equipped with a Leica 63×/1.40 Oil HC PL APO objective (Leica Microsystems, Wetzlar, Germany). Imaging was carried out using the GFP filter set. Mean fluorescence intensity was calculated as the average of regions of interest by using IMAGEJ software (National Institutes of Health, Bethesda, MD, USA).

Transfections

To determine LC-3 puncta formation, Caco-2 cells were plated in 6-well plates and cells at the 0th day or 10th day after reaching confluency were transiently transfected for 48 h with 2.5 μg of an EGFP-LC3 vector. For microscopy, the cells were fixed in 4% formaldehyde for 15 min at room temperature and permeabilized in 1× PBS containing 0.3% Triton X-100 for 10 min at room temperature. The cells were collected, resuspended in mounting medium (Slow Fade Gold antifade reagent; Invitrogen), and taken on glass slides for visualization under a fluorescence microscope (Leica). To quantify LC3 puncta formation, 100–200 GFP-positive cells with at least five green dots per cell were counted for each replicate. The ratio of cells with five or more puncta (representing autophagic cells) to the total number of GFP-positive cells was calculated and presented as a graph. The EGFP-LC3 vector was kindly provided by Tamotsu Yoshimori [65].

Chromatin immunoprecipitation (ChIP)

The culture medium from proliferating or differentiated Caco-2 cells was removed, and the cells were fixed with ChIP-IT® Fixation Buffer (Active Motif, Carlsbad, CA, USA) for 15 min according to the manufacturer's protocol. To stop the fixation reaction, 125 mM glycine was added to the existing culture media and incubated for 5 min. The cells were then washed twice with 1× PBS at room temperature. After aspirating PBS completely, cross-linked cells were gently detached in ice-cold 1× PBS containing protease inhibitors on ice, using a scraper. After centrifugation at 13 000 ***g*** for 1 min at 4 °C, the pellets were then frozen in liquid nitrogen and stored at −80 °C or used immediately. For sonication, cells were suspended in ChIP SDS lysis buffer (1.0% SDS, 10 mM EDTA, 50 mM Tris/HCl pH 8.1, 1× protease inhibitor cocktail, 1 mM PMSF) on ice for 10 min, and then sonicated using an ultrasonic cup horn sonicator (Q700 QSonica®; Newtown, CT, USA) with a pulse mode of 30-s ON and 30-s OFF for 20 min, while output intensity was 100%. Following sonication, the samples were centrifuged at 14 000 ***g*** for 15 min at 4 °C and the supernatants were collected to a new tube. DNA amount was determined, and 50 μg of chromatin was diluted 10 times in ChIP dilution buffer (0.01% SDS, 1.1% Triton X, 1.2 mM EDTA, 16.7 mM Tris/HCl pH 8.1, 167 mM NaCl, 1× protease inhibitor cocktail, 1 mM PMSF) followed by preclearing with 10 : 1 v/v chromatin : Protein A/G PLUS-Agarose Beads (Santa Cruz Biotechnology, Dallas, TX, USA) for 2 h at 4 °C, using a rotator. Samples were centrifuged at 1800 ***g*** for 2 min at 4 °C, and the supernatants were collected in a new tube. 10% v/v of supernatant was saved in a fresh tube to be used as 'input'. Fifty microgram of chromatin samples was rotated o/n at 4 °C with 5 μg of HNF4α (Thermo Fisher Scientific, K9218, cat no: MA1-199) or CDX2 antibodies (Abcam, Cambridge, UK, Cat No: ab15258) or corresponding IgG antibodies (Santa Cruz Biotechnology, Cat No: sc:2028 for HNF4α and sc:2025 for CDX2). The day after, 80 μL of Protein A/G PLUS-Agarose beads (Santa Cruz Biotechnology, Cat No: sc-2003) was added to each sample (IgG or specific antibody), and the samples were incubated with the beads mixture at 4 °C under rotary agitation for 2 h. Following centrifugation at 1800 ***g***, 4 °C for 2 min, the supernatants were discarded and the beads were washed twice with low salt buffer (0.1% SDS, 1% Triton X-100, 2 mM EDTA, 20 mM Tris/HCl pH 8.1, 150 mM NaCl), twice with high salt buffer (0.1% SDS, 1% Triton X-100, 2 mM EDTA, 20 mM Tris/HCl pH 8.1, 500 mM NaCl), once with LiCl buffer (0.25 M LiCl, 1% IGEPAL-CA630, 1% deoxycholic acid, 1 mM EDTA, 10 mM Tris pH 8.1), and twice with TE buffer (10 mM Tris/HCl, 1 mM EDTA, pH 8.0). After washing, elution buffer containing 1% SDS and 0.1 M $NaHCO_3$ was added onto the beads to elute the protein complex from the antibody by incubating at room temperature for 15 min with rotation. Five molar of NaCl was added to the eluates, and protein–DNA crosslinks were reversed by heating at 65 °C for 4 h. Ten millimolar EDTA, 40 mM Tris/HCl pH 6.5, and proteinase K containing eluates were incubated at 45 °C for 1 h followed by column purification of DNA using ChIP DNA Clean & Concentrator Kit (Zymo Research, Irvine, CA, USA). The purified DNA samples were used in qRT-PCRs. The ChIP primers used in the qRT-PCRs are given in Table S7.

In silico analyses

The raw files for GSE17538 were downloaded using the GEOquery [66] package from Bioconductor (https://www.bioconductor.org/install/). Raw data were then normalized using GCRMA [67] and annotated with hgu133plus2.db [68] packages, respectively. Afterward, cancer samples were classified into poor (n = 28), moderate (n = 163), and well-differentiated (n = 16) based on the clinical data available in ArrayExpress database (https://www.ebi.ac.uk/arrayexpress/experiments/). Probes for the genes of interest were extracted from the expression matrix, and the highest expressing ones were used for further graphical and statistical analysis. All statistical tests were carried out on R Programming Language version 3.5.1 [69].

The normalized data as well as probe annotation file for GSE84742 were downloaded from ArrayExpress database (https://www.ebi.ac.uk/arrayexpress/experiments/). Individual files were converted into an overall data frame using basic R packages, and probes were matched to their respective symbols using dplyr package [70].

Differential expression analysis for GSE11759 *Hnf4α* wild-type vs knockout was performed using limma package [71], and the probes representing genes for ER stress and autophagy were selected based on the information provided by the annotation package. Selection criteria were based on P-value < 0.05 and when multiple probes were present, the most significant ones were taken into consideration. All statistical tests indicated on respective figures were carried out on R Programming Language version 3.5.3 [69].

For HNF4α ChIP-Sequencing dataset (GSE23436) analysis, MACS2 peak calling results for GSM575228 (proliferating cells) and GSM575229 (differentiated cells) were obtained from GEO database [32]. For the annotation of the peaks 2000 bp upstream region was obtained from UCSC Genome Browser [72] and merged with GALAXY tool [73]. PantherDB was used for the enrichment analysis of obtained genes [74].

For XBP1 and ATF6 enrichment analysis from HNF4α ChIP-Sequencing dataset (GSE23436), SRA files were downloaded and reads were mapped to hg18 genome assembly using bowtie version 2.3.3 [75]. MACS2 was used for peak calling [76]. For the annotation of the peaks, 2000 bp upstream region was obtained from UCSC Genome Browser [72] and merged with GALAXY tool [73]. Reads were visualized with EaSeq [77].

To analyze the GSE69333 dataset, raw sequencing files were obtained for GSM1697907 (day 0), GSM1697908 (day 4), GSM1697909 (day 12), and GSM16979010 (day 15) with SRA toolkit. Reads were mapped to hg19 genome using bowtie2 version 2.3.3 [75]. Peak caller software MACS2 [76] was used to identify enriched peaks against the day 0 sequence. Five thousand base pair upstream and downstream region of TSS data was obtained from UCSC Genome Browser [72] and merged with GALAXY tool [73]. GSM1697907 (day 0) cells were used as control for peak calling. The up- and downstream regions are shown with different colors. Peaks with lowest q value were reported. Reads were visualized with EaSeq [77].

Statistical analyses

All experiments were repeated at least three times, and data are expressed as mean ± standard error of mean (SEM). Statistical analyses between experimental results were based on unpaired t-test, and GRAPHPAD (Prism version 6.00 for Windows, GraphPad Software, La Jolla, CA, USA) was used for data analyses and for the generation of graphs, unless otherwise indicated.

Acknowledgements

This work was funded from TÜBİTAK Project No. 114S937 to SB, 113S985 to AA, and Bilecik Şeyh Edebali University Scientific Research Fund, Project No: 2018-01.BŞEÜ.12-01 to ST. Dr Tamotsu Yoshimori from the Department of Cell Biology, National Institute for Basic Biology, Okazaki, Japan, is acknowledged for sharing the GFP-LC-3 plasmid, and Dr Ebru Erbay and Dr Devrim Gözüaçık are gratefully acknowledged for sharing many reagents. Dr Ozlen Konu is gratefully acknowledged for useful discussions. Ezgi Güleç and Hazal Hüsnügil are acknowledged for helping in postconfluent culturing of SW-480, T84, and Caco-2 cells.

Conflict of interest

The authors declare no conflict of interest.

Author contributions

ST performed the experimental work with contributions from ASM and analyzed and interpreted the data. AGK and IS carried out the bioinformatics analyses; GG and AA carried out the staining of TMA. SB designed and supervised the research, interpreted the data, and wrote the manuscript with ST.

References

1 Delgado ME, Grabinger T & Brunner T (2016) Cell death at the intestinal epithelial front line. *FEBS J* **283**, 2701–2719.
2 Simons BD & Clevers H (2011) Stem cell self-renewal in intestinal crypt. *Exp Cell Res* **317**, 2719–2724.
3 Stegmann A, Hansen M, Wang Y, Larsen JB, Lund LR, Ritie L, Nicholson JK, Quistorff B, Simon-Assmann P, Troelsen JT *et al.* (2006) Metabolome,

transcriptome, and bioinformatic cis-element analyses point to HNF-4 as a central regulator of gene expression during enterocyte differentiation. *Physiol Genomics* **27**, 141–155.
4 Kaser A, Flak MB, Tomczak MF & Blumberg RS (2011) The unfolded protein response and its role in intestinal homeostasis and inflammation. *Exp Cell Res* **317**, 2772–2779.
5 He Y, Sun S, Sha H, Sha H, Liu Z, Yang L, Xue Z, Chen H & Qi L (2010) Emerging roles for XBP1, a sUPeR transcription factor. *Gene Expr* **15**, 13–25.
6 Tsuru A, Imai Y, Saito M & Kohno K (2016) Novel mechanism of enhancing IRE1α-XBP1 signalling via the PERK-ATF4 pathway. *Sci Rep* **6**, 24217.
7 Heijmans J, van Lidth de Jeude JF, Koo B-K, Rosekrans SL, Wielenga MCB, van de Wetering M, Ferrante M, Lee AS, Onderwater JJM, Paton JC *et al.* (2013) ER stress causes rapid loss of intestinal epithelial stemness through activation of the unfolded protein response. *Cell Rep* **3**, 1128–1139.
8 Yao HS, Wang J, Zhang XP, Wang LZ, Wang Y, Li XX, Jin KZ, Hu ZQ & Wang WJ (2016) Hepatocyte nuclear factor 4α suppresses the aggravation of colon carcinoma. *Mol Carcinog* **55**, 458–472.
9 Moore BD, Jin RU, Lo H, Jung M, Wang H, Battle MA, Wollheim CB, Urano F & Mills JC (2016) Transcriptional regulation of X-Box-binding protein One (XBP1) by hepatocyte nuclear factor 4- (HNF4-) Is vital to beta-cell function. *J Biol Chem* **291**, 6146–6157.
10 Moore BD, Khurana SS, Huh WJ & Mills JC (2016) Hepatocyte nuclear factor 4α is required for cell differentiation and homeostasis in the adult mouse gastric epithelium. *Am J Physiol Gastrointest Liver Physiol* **311**, G267–G275.
11 Smith M & Wilkinson S (2017) ER homeostasis and autophagy. *Essays Biochem* **61**, 625–635.
12 Tanida I, Ueno T & Kominami E (2004) LC3 conjugation system in mammalian autophagy. *Int J Biochem Cell Biol* **36**, 2503–2518.
13 Tunçer S & Banerjee S (2019) Determination of autophagy in the caco-2 spontaneously differentiating model of intestinal epithelial cells. *Methods Mol Biol* **1854**, 55–70.
14 Pankiv S, Clausen TH, Lamark T, Brech A, Bruun JA, Outzen H, Øvervatn A, Bjørkøy G & Johansen T (2007) p62/SQSTM1 binds directly to Atg8/LC3 to facilitate degradation of ubiquitinated protein aggregates by autophagy. *J Biol Chem* **282**, 24131–24145.
15 Zaffagnini G, Savova A, Danieli A, Romanov J, Tremel S, Ebner M, Peterbauer T, Sztacho M, Trapannone R, Tarafder AK *et al.* (2018) p62 filaments capture and present ubiquitinated cargos for autophagy. *EMBO J* **37**, e98308.
16 Bel S, Pendse M, Wang Y, Li Y, Ruhn KA, Hassell B, Leal T, Winter SE, Xavier RJ & Hooper LV (2017) Paneth cells secrete lysozyme via secretory autophagy during bacterial infection of the intestine. *Science* **357**, 1047–1052.
17 Pedersen G (2015) Development, validation and implementation of an *in vitro* model for the study of metabolic and immune function in normal and inflamed human colonic epithelium. *Dan Med J* **62**, B4973.
18 Benjamin JL, Sumpter R, Levine B & Hooper LV (2013) Intestinal epithelial autophagy is essential for host defense against invasive bacteria. *Cell Host Microbe* **13**, 723–734.
19 Nighot PK, Hu CAA & Ma TY (2015) Autophagy enhances intestinal epithelial tight junction barrier function by targeting claudin-2 protein degradation. *J Biol Chem* **290**, 7234–7246.
20 San Roman AK, Aronson BE, Krasinski SD, Shivdasani RA & Verzi MP (2015) Transcription factors GATA4 and HNF4A control distinct aspects of intestinal homeostasis in conjunction with transcription factor CDX2. *J Biol Chem* **290**, 1850–1860.
21 Boyd M, Bressendorff S, Møller J, Olsen J & Troelsen JT (2009) Mapping of HNF4alpha target genes in intestinal epithelial cells. *BMC Gastroenterol* **9**, 68.
22 Buhrke T, Lengler I & Lampen A (2011) Analysis of proteomic changes induced upon cellular differentiation of the human intestinal cell line Caco-2. *Dev Growth Differ* **53**, 411–426.
23 Kitadai Y, Radinsky R, Bucana CD, Takahashi Y, Xie K, Tahara E & Fidler IJ (1996) Regulation of carcinoembryonic antigen expression in human colon carcinoma cells by the organ microenvironment. *Am J Pathol* **149**, 1157–1166.
24 Babeu JP & Boudreau F (2014) Hepatocyte nuclear factor 4-alpha involvement in liver and intestinal inflammatory networks. *World J Gastroenterol* **20**, 22–30.
25 Babeu J-P, Jones C, Geha S, Carrier JC & Boudreau F (2018) P1 promoter-driven HNF4α isoforms are specifically repressed by β-catenin signaling in colorectal cancer cells. *J Cell Sci* **131**, 1–13.
26 Ko HL, Zhuo Z & Ren EC (2019) HNF4α combinatorial isoform heterodimers activate distinct gene targets that differ from their corresponding homodimers. *Cell Rep* **26**, 2549–2577.e3.
27 Lili LN, Farkas AE, Gerner-Smidt C, Overgaard CE, Moreno CS, Parkos CA, Capaldo CT & Nusrat A (2016) Claudin-based barrier differentiation in the colonic epithelial crypt niche involves Hopx/Klf4 and Tcf7l2/Hnf4-α cascades. *Tissue Barriers* **4**, e1214038.
28 Ancey PB, Ecsedi S, Lambert MP, Talukdar FR, Cros MP, Glaise D, Narvaez DM, Chauvet V, Herceg Z, Corlu A *et al.* (2017) TET-Catalyzed 5-hydroxymethylation precedes HNF4A promoter choice during differentiation of bipotent liver progenitors. *Stem Cell Rep* **9**, 264–278.
29 Sharif J, Endo TA, Toyoda T & Koseki H (2010) Divergence of CpG island promoters: a consequence or cause of evolution? *Dev Growth Differ* **52**, 545–554.

30 Chapman CG, Mariani CJ, Wu F, Meckel K, Butun F, Chuang A, Madzo J, Bissonnette MB, Kwon JH & Godley LA (2015) TET-catalyzed 5-hydroxymethylcytosine regulates gene expression in differentiating colonocytes and colon cancer. *Sci Rep* **5**, 17568.
31 Niv Y, Byrd JC, Ho SB, Dahiya R & Kim YS (1992) Mucin synthesis and secretion in relation to spontaneous differentiation of colon cancer cells *in vitro*. *Int J Cancer* **50**, 147–152.
32 Verzi MP, Shin H, He HH, Sulahian R, Meyer CA, Montgomery RK, Fleet JC, Brown M, Liu XS & Shivdasani RA (2010) Differentiation-specific histone modifications reveal dynamic chromatin interactions and partners for the intestinal transcription factor CDX2. *Dev Cell* **19**, 713–726.
33 Smith JJ, Deane NG, Wu F, Merchant NB, Zhang B, Jiang A, Lu P, Johnson JC, Schmidt C, Bailey CE *et al.* (2010) Experimentally derived metastasis gene expression profile predicts recurrence and death in patients with colon cancer. *Gastroenterology* **138**, 958–968.
34 Darsigny M, Babeu JP, Dupuis AA, Furth EE, Seidman EG, Lévy É, Verdu EF, Gendron FP & Boudreau F (2009) Loss of hepatocyte-nuclear-factor-4α affects colonic ion transport and causes chronic inflammation resembling inflammatory bowel disease in mice. *PLoS ONE* **4**, e7609.
35 Krebs J, Agellon LB & Michalak M (2015) Ca2 + homeostasis and endoplasmic reticulum (ER) stress: an integrated view of calcium signaling. *Biochem Biophys Res Commun* **460**, 114–121.
36 Fogarty S, Ross FA, Vara Ciruelos D, Gray A, Gowans GJ & Hardie DG (2016) AMPK causes cell cycle arrest in LKB1-deficient cells via activation of CAMKK2. *Mol Cancer Res* **14**, 683–695.
37 Xu J, Ji J & Yan XH (2012) Cross-talk between AMPK and mTOR in regulating energy balance. *Crit Rev Food Sci Nutr* **52**, 373–381.
38 Sheshadri N, Catanzaro JM, Bott AJ, Sun Y, Ullman E, Chen EI, Pan JA, Wu S, Crawford HC, Zhang J *et al.* (2014) SCCA1/SERPINB3 promotes oncogenesis and epithelial-mesenchymal transition via the unfolded protein response and IL6 signaling. *Cancer Res* **74**, 6318–6329.
39 Papaioannou A, Higa A, Jégou G, Jouan F, Pineau R, Saas L, Avril T, Pluquet O & Chevet E (2018) Alterations of EDEM1 functions enhance ATF6 pro-survival signaling. *FEBS J* **285**, 4146–4164.
40 Hong M, Luo S, Baumeister P, Huang JM, Gogia RK, Li M & Lee AS (2004) Underglycosylation of ATF6 as a novel sensing mechanism for activation of the unfolded protein response. *J Biol Chem* **279**, 11354–11363.
41 Groulx JF, Khalfaoui T, Benoit YD, Bernatchez G, Carrier JC, Basora N & Beaulieu JF (2012) Autophagy is active in normal colon mucosa. *Autophagy* **8**, 893–902.
42 García-Lorenzo A, Rodríguez-Piñeiro AM, Rodríguez-Berrocal FJ, de la Cadena MP & Martínez-Zorzano VS (2012) Changes on the Caco-2 secretome through differentiation analyzed by 2-D differential in-gel electrophoresis (DIGE). *Int J Mol Sci* **13**, 14401–14420.
43 Klose RJ & Bird AP (2006) Genomic DNA methylation: the mark and its mediators. *Trends Biochem Sci* **31**, 89–97.
44 Ehrlich M & Ehrlich KC (2014) DNA cytosine methylation and hydroxymethylation at the borders. *Epigenomics* **6**, 563–566.
45 Bettigole SE, Lis R, Adoro S, Lee AH, Spencer LA, Weller PF & Glimcher LH (2015) The transcription factor XBP1 is selectively required for eosinophil differentiation. *Nat Immunol* **16**, 829–837.
46 Tsuchiya M, Koizumi Y, Hayashi S, Hanaoka M, Tokutake Y & Yonekura S (2017) The role of unfolded protein response in differentiation of mammary epithelial cells. *Biochem Biophys Res Commun* **484**, 903–908.
47 Lee AH, Chu GC, Iwakoshi NN & Glimcher LH (2005) XBP-1 is required for biogenesis of cellular secretory machinery of exocrine glands. *EMBO J* **24**, 4368–4380.
48 Wu J & Kaufman RJ (2006) From acute ER stress to physiological roles of the unfolded protein response. *Cell Death Differ* **13**, 374–384.
49 Han J & Kaufman RJ (2016) The role of ER stress in lipid metabolism and lipotoxicity. *J Lipid Res* **57**, 1329–1338.
50 Hillary RF & Fitzgerald U (2018) A lifetime of stress: ATF6 in development and homeostasis. *J Biomed Sci* **25**, 48.
51 Kroeger H, Grimsey N, Paxman R, Chiang WC, Plate L, Jones Y, Shaw PX, Trejo JA, Tsang SH, Powers E *et al.* (2018) The unfolded protein response regulator ATF6 promotes mesodermal differentiation. *Sci Signal* **11**, 1–13.
52 Yamamoto K, Takahara K, Oyadomari S, Okada T, Sato T, Harada A & Mori K (2010) Induction of liver steatosis and lipid droplet formation in ATF6 - knockout mice burdened with pharmacological endoplasmic reticulum stress. *Mol Biol Cell* **21**, 2975–2986.
53 Sica V, Galluzzi L, Bravo-San Pedro JM, Izzo V, Maiuri MC & Kroemer G (2015) Organelle-specific initiation of autophagy. *Mol Cell* **59**, 522–539.
54 Kania E, Pająk B & Orzechowski A (2015) Calcium homeostasis and ER stress in control of autophagy in cancer cells. *Biomed Res Int* **2015**, 352794.
55 Asano J, Sato T, Ichinose S, Kajita M, Onai N, Shimizu S & Ohteki T (2017) Intrinsic autophagy is required for the maintenance of intestinal stem cells and for irradiation-induced intestinal regeneration. *Cell Rep* **20**, 1050–1060.
56 Nagy P, Sándor GO & Juhász G (2018) Autophagy maintains stem cells and intestinal homeostasis in *Drosophila*. *Sci Rep* **20**, 1050–1060.

57 Mizushima N (2009) Physiological functions of autophagy. *Curr Top Microbiol Immunol* **335**, 71–84.
58 Wang L, Ye X & Zhao T (2019) The physiological roles of autophagy in the mammalian life cycle. *Biol Rev* **94**, 503–516.
59 Singh R, Kaushik S, Wang Y, Xiang Y, Novak I, Komatsu M, Tanaka K, Cuervo AM & Czaja MJ (2009) Autophagy regulates lipid metabolism. *Nature* **458**, 1131–1135.
60 Lopes F, Keita ÅV, Saxena A, Reyes JL, Mancini NL, Al Rajabi A, Wang A, Baggio CH, Dicay M, Van Dalen R *et al.* (2018) ER-stress mobilization of death-associated protein kinase-1- dependent xenophagy counteracts mitochondria stress-induced epithelial barrier dysfunction. *J Biol Chem* **293**, 3073–3087.
61 Lambert E, Babeu J-P, Simoneau J, Lévesque D, Jolibois É, Scott M, Boudreau F & Boisvert F-M (2019) Human hepatocyte nuclear factor 4- α encodes isoforms with distinct transcriptional functions. *bioRxiv*, 819–820. "[PREPRINT]".
62 Pinto M, Robine-Leon S, Appay M-D, Kedinger M, Triadou N, Dussaulx E, Lacroix B, Simon-Assmann P, Haffen K, Fogh J *et al.* (1983) Enterocyte-like differentiation and polarization of the human colon carcinoma cell line Caco-2 in culture. *Biol Cell* **47**, 323–330.
63 Pfaffl MW (2001) A new mathematical model for relative quantification in real-time RT-PCR. *Nucleic Acids Res* **29**, 45e–45.
64 Bustin SA, Benes V, Garson JA, Hellemans J, Huggett J, Kubista M, Mueller R, Nolan T, Pfaffl MW, Shipley GL *et al.* (2009) The MIQE guidelines: minimum information for publication of quantitative real-time PCR experiments. *Clin Chem* **55**, 611–622.
65 Kabeya Y, Mizushima N, Ueno T, Yamamoto A, Kirisako T, Noda T, Kominami E, Ohsumi Y, Yoshimori T (2000) LC3, a mammalian homologue of yeast Apg8p, is localized in autophagosome membranes after processing. *EMBO J* **19**, 5720–5728.
66 Davis S (2014) Using the GEOquery Package.
67 Wu J, Gentry RIwcfJMJ (2019) gcrma: Background Adjustment Using Sequence Information. R package version 2.58.0.
68 Carlson M (2016). hgu133plus2.db: Affymetrix Human Genome U133 Plus 2.0 Array annotation data (chip hgu133plus2). R package version 3.2.3.
69 Venables WN, Smith DM & the R Development Core Team (2019) Notes on R: A Programming Environment for Data Analysis and Graphics Version 3.6.1 (2019-07-05).
70 Wickham H, François R, Henry L & Müller K (2018) Package "dplyr". CRAN.
71 Ritchie ME, Phipson B, Wu D, Hu Y, Law CW, Shi W & Smyth GK (2015) limma powers differential expression analyses for RNA-sequencing and microarray studies. *Nucleic Acids Res* **43**, e47.
72 Karolchik D (2004) The UCSC Table Browser data retrieval tool. *Nucleic Acids Res* **32**, 493D–496.
73 Afgan E, Baker D, Batut B, Van Den Beek M, Bouvier D, Ech M, Chilton J, Clements D, Coraor N, Grüning BA *et al.* (2018) The Galaxy platform for accessible, reproducible and collaborative biomedical analyses: 2018 update. *Nucleic Acids Res* **46**, W537–W544.
74 Mi H, Huang X, Muruganujan A, Tang H, Mills C, Kang D & Thomas PD (2017) PANTHER version 11: expanded annotation data from Gene Ontology and Reactome pathways, and data analysis tool enhancements. *Nucleic Acids Res* **45**, D183–D189.
75 Langmead B & Salzberg SL (2012) Fast gapped-read alignment with Bowtie 2. *Nat Methods* **9**, 357–359.
76 Zhang Y, Liu T, Meyer CA, Eeckhoute J, Johnson DS, Bernstein BE, Nussbaum C, Myers RM, Brown M, Li W *et al.* (2008) Model-based analysis of ChIP-Seq (MACS). *Genome Biol* **9**, R137.
77 Lerdrup M, Johansen JV, Agrawal-Singh S & Hansen K (2016) An interactive environment for agile analysis and visualization of ChIP-sequencing data. *Nat Struct Mol Biol* **23**, 349–357.

Supporting information

Additional supporting information may be found online in the Supporting Information section at the end of the article.

Table S1. Human HNF4α transcripts (modified from Lambert *et al.*, 2019).

Table S2. Hydroxymethylation of HNF4α gene during spontaneous differentiation of colon cancer cells: Cytosine hydroxymethylation patterns of differentiated and undifferentiated T84 colon cancer cells were investigated using a publicly available dataset (GSE69333).

Table S3. Coordinates for HNF4α occupancy at the promoter of XBP1 and PARK2: An increase in fold enrichment was seen for occupancy of the XBP1 promoter in the differentiated cells compared to the undifferentiated cells.

Table S4. Major parameters of the immunohistochemistry assays.

Table S5. Primary and secondary antibodies used for western blot.

Table S6. mRNA expression primers used in the study: Primer sequences, annealing temperatures of the primers, amplified product sizes and target mRNA IDs (GRCh38.p7 Primary Assembly, NCBI) are given.

Table S7. ChIP primers used to quantify enriched genomic regions using qRT-PCR: Primer sequences, annealing temperatures of the primers, and amplified product sizes are included.